De Novo Missense Variants in WDR37 Cause a Severe Multisystemic Syndrome

Linda M. Reis,[1,6] Elena A. Sorokina,[1,6] Samuel Thompson,[1] Sanaa Muheisen,[1] Milen Velinov,[2] Carlos Zamora,[3] Arthur S. Aylsworth,[4] and Elena V. Semina[1,5,*]

While genetic causes are known for many syndromes involving developmental anomalies, a large number of individuals with overlapping phenotypes remain undiagnosed. Using exome-sequencing analysis and review of matchmaker databases, we have discovered four de novo missense variants predicted to affect the N-terminal region of WDR37—p.Ser119Phe, p.Thr125Ile, p.Ser129Cys, and p.Thr130Ile—in unrelated individuals with a previously unrecognized syndrome. Features of WDR37 syndrome include the following: ocular anomalies such as corneal opacity/Peters anomaly, coloboma, and microcornea; dysmorphic facial features; significant neurological impairment with structural brain defects and seizures; poor feeding; poor post-natal growth; variable skeletal, cardiac, and genitourinary defects; and death in infancy in one individual. WDR37 encodes a protein of unknown function with seven predicted WD40 domains and no previously reported human pathogenic variants. Immunocytochemistry and western blot studies showed that wild-type WDR37 is localized predominantly in the cytoplasm and mutant proteins demonstrate similar protein levels and localization. CRISPR-Cas9-mediated genome editing generated zebrafish mutants with novel missense and frameshift alleles: p.Ser129Phe, p.Ser129Cys (which replicates one of the human variants), p.Ser129Tyr, p.Lys127Cysfs, and p.Gln95Argfs. Zebrafish carrying heterozygous missense variants demonstrated poor growth and larval lethality, while heterozygotes with frameshift alleles survived to adulthood, suggesting a potential dominant-negative mechanism for the missense variants. RNA-seq analysis of zebrafish embryos carrying a missense variant detected significant upregulation of cholesterol biosynthesis pathways. This study identifies variants in WDR37 associated with human disease and provides insight into its essential role in vertebrate development and possible molecular functions.

Developmental ocular conditions such as Peters anomaly and coloboma are often accompanied by additional syndromic anomalies.[1,2] Some syndromes are well defined with known genetic causes, including Peters-plus syndrome (B3GLCT [MIM: 261540]),[3] CHARGE syndrome (CHD7 [MIM: 214800]),[4] Temtamy syndrome (C12orf57 [MIM: 218340]),[5] and Walker-Warburg syndrome (POMT1 [MIM: 236670], POMT2 [MIM: 613150], and other genes).[6,7] Many similarly affected individuals, however, have features that partially overlap these known syndromes and remain causally unexplained.[1,8,9]

In this study we report human disease-causing variants in WDR37 (WD repeat domain 37; GenBank: NM_014023.3) in several individuals with previously uncharacterized syndromic malformations. This human study was approved by the Institutional Review Board of the Children's Hospital of Wisconsin with written informed consent obtained for participation and publication for every participant. Detailed case descriptions are provided in the Supplemental Note. Exome sequencing was performed (Table S1) and analyzed as previously reported[1] with in silico predictions of the effect of missense variants obtained from dbNSFP for SIFT, PolyPhen2, MutationTaster, MutationAssessor, and FATHMM MKL.

Trio analysis in individual 1 (Figure 1) and his parents identified a de novo missense variant in WDR37, c.356C>T (p.Ser119Phe) (Figure S1). The variant is not present in gnomAD and is predicted damaging by all five in silico programs. Review of exome data from other individuals with unexplained syndromic eye disorders[1,9] enrolled in our study identified an additional de novo missense variant in WDR37 in individual 2, c.389C>T (p.Thr130Ile) (Figures 1 and S1), also not present in gnomAD and predicted damaging by all five programs. Both affected individuals were referred to the study with possible clinical diagnoses of either Peters plus or Walker-Warburg syndromes. Both were non-verbal with limited or no ambulation and seizure onset shortly after birth and showed overlapping clinical features including ocular anomalies (corneal opacity/Peters anomaly, microcornea, coloboma, and lens defects), dysmorphic craniofacial features (microcephaly, thin upper lip, broad nasal bridge, abnormal ears), structural brain anomalies (Dandy-Walker spectrum malformation, abnormal myelination), congenital heart defects, skeletal anomalies (severe short stature, scoliosis, contractures), genitourinary anomalies (cryptorchidism, micropenis, hypoplastic uterus, and kidney defects), and feeding disorders (poor intake/feeding intolerance) (Table 1, Supplemental
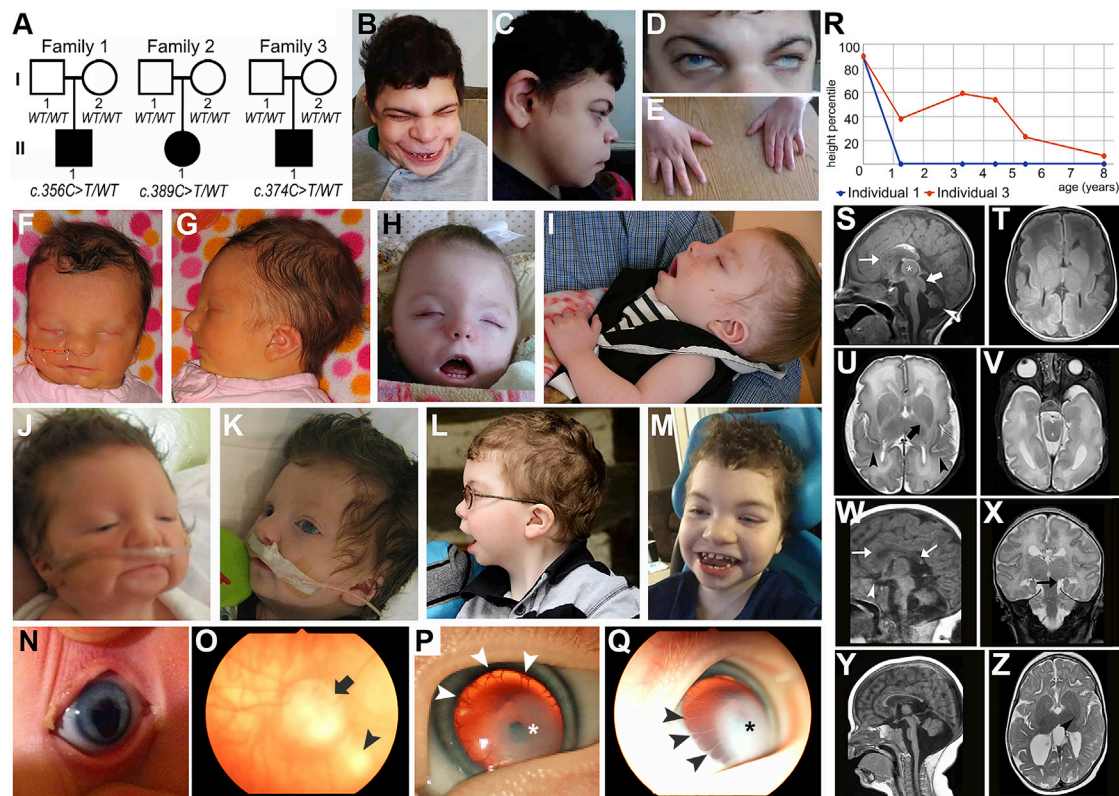
Figure 1. Images of Affected Individuals

(A) Pedigrees from individuals 1–3 with *WDR37* variants indicated.

(B–E) Photographs of individual 1 at age 30 years showing microcephaly, broad nasal bridge, thin upper lip, protruding jaw, and ear anomalies (B, C); eye anomalies including corneal opacity and microcornea (D); and small hands (E).

(F–I) Photographs of individual 2 at age 4 days (F, G) and 22 months (H, I) showing microcephaly, apparent hypertelorism, broad nasal bridge, thin upper lip, micrognathia, and ear anomalies.

(J–M) Facial photographs of individual 3 at ages 1 day (J), 3 weeks (K), 5 years (L), and 8 years (M) showing microcephaly, broad nasal bridge, thin upper lip, broad chin, and abnormal ears.

(N–Q) Ocular images of individual 3 taken at age 5 months showing right eye with iris coloboma (N) and mild inferior optic nerve dysplasia (arrow) and chorioretinal coloboma (arrowhead) (O) and left eye (pupil dilated) with Peters anomaly (central corneal leukoma [*] and iris adhesions to the endothelium [arrowheads]), iris coloboma, and microcornea (P–Q).

(R) Height centiles for Individuals 1 and 3 by year of age, showing normal birth length but decreasing height centiles over time.

(S–V) Brain MRI images from individual 2 at age 5 days. Sagittal noncontrast T1 image (S) shows a prominent massa intermedia (asterisk), large midbrain tectum (large white arrow), small pons, hypoplastic corpus callosum (thin white arrow) with a small rostrum and splenium, bright pericallosal lipoma, and Dandy-Walker variant with vermian hypoplasia (white arrowhead) and dilation of the fourth ventricle. Axial noncontrast T1 (T) demonstrates an abnormal gyral pattern and abnormal configuration of the basal ganglia. Axial T2 images (U and V) show abnormal diffuse white matter hyperintensity (decreased myelination), particularly notable in the posterior limb of the internal capsule (large black arrow) and dysplastic, thickened cortex in the sylvian fissures (black arrowheads), as well as left microphthalmia with aphakia and small, incompletely inverted hippocampi.

(W–Z) Brain MRI images from individual 3. Sagittal noncontrast T1 image at age 11 days (W) shows thinned corpus callosum (white arrows), enlarged massa intermedia, mildly prominent midbrain tectum, and a Dandy-Walker variant with hypoplastic cerebellar vermis. The optic chiasm and nerves appear atrophic (white arrowhead) and the pituitary gland is small with absent posterior bright spot. Concurrent coronal T2 image (X) shows simplified gyral pattern, diffuse white matter hyperintensity, and small and incompletely inverted hippocampi (black arrow). Follow-up sagittal noncontrast T1 at age 11 months (Y) shows increased dilation of the posterior fossa and relatively small brainstem while the concurrent T2 image (Z) shows delayed myelination of the posterior limb of the internal capsule (black arrowhead) and extensive white matter volume loss with enlarged ventricles. Detailed clinical and MRI descriptions are included in the Supplemental Note.

Note). Individual 1 is now 30 years old; individual 2 died at age 22 months from respiratory failure due to pneumonia and cardiac anomalies. Several other rare variants of uncertain significance were also identified within the exome data, but based on testing of family members, general population data, and *in silico* predictions, all are considered likely benign (Table S2).

A search of the matchmaker database MyGene2 (see Web Resources) identified two additional individuals with *de novo*, novel variants in *WDR37* within the same region; both variants were similarly predicted damaging by all five *in silico* programs. Individual 3, with a c.374C>T (p.Thr125Ile) variant, was subsequently enrolled in the study for confirmation of the variant and detailed review

Table 1. Clinical Features of Affected Individuals with *WDR37* Variants

	Individual 1	Individual 2	Individual 3[a]	Individual 4[b]
De novo WDR37 variant	c.356C>T (p.Ser119Phe)	c.389C>T (p.Thr130Ile)	c.374C>T (p.Thr125Ile)	c.386C>G (p.Ser129Cys)
Age	30 years	22 months (dec)	8 years	U
Ocular Features				
Microcornea*	+	+	+	U
Corneal opacity/Peters*[b]	+	+	+	U
Coloboma*	?	+	+	+
Other	glaucoma, juvenile cataract	aphakia, ONH, retinal dysplasia	cataract, ONH, retinal dysplasia	U
Craniofacial/Neck Features				
Microcephaly*	+	+	+	+
Protruding jaw/broad chin	+	−	+	U
Thin upper lip*	+	+	+	U
Broad nasal bridge*	+	+	+	+
Ear anomalies*	+	+	+	+
Excess nuchal skin/webbed neck	U	+	+	U
Other	arched eyebrows	hearing loss, hypertelorism	hearing loss	hypertelorism
Neurological Anomalies				
Seizures*	+	+	+	+
Dandy-Walker variant*	+	+	+	?
Delayed myelination/dysmyelination*	+	+	+	U
Abnormal gyration pattern	−	+	+	U
Absent/hypoplastic corpus callosum	−	+	+	U
Non-verbal, severe global delay*	+	+	+	?
Cardiovascular Anomalies				
Septal defect (ASD/VSD)	+	+	−	?
Patent ductus arteriosus*	+	+	+	?
Genitourinary Anomalies				
Cryptorchidism, micropenis	+	NA (female)	+	U
Hypoplastic uterus	NA (male)	+	NA (male)	U
Hydronephrosis/ureterocele	−	+	+	U
Other	incomp. puberty	renal dysplasia	−	U
Skeletal/Spinal Anomalies				
Short stature*	+	+	−	+
Spine anomalies	+	+	−	U
Syndactyly	−	+	+	U
Contractures*	+	+	+	U
Other	hip dislocation, pectus anomaly	−	hip dislocation, coxa valga	U

(Continued on next page)

Table 1. Continued

	Individual 1	Individual 2	Individual 3[a]	Individual 4[b]
Gastrointestinal				
Feeding disorder*	+	+	+	U
Other	−	pancreatic lipomatosis	small stomach, malrotation, GERD	U

Abbreviations: U, unknown; ?, features possibly consistent with this diagnosis but insufficient details available; dec, deceased; ONH, optic nerve hypoplasia; GERD, gastroesophageal reflux disease; NA, not applicable; features with asterisk (*) are observed in three or more affected individuals; GenBank: NM_014023.3 used as reference sequence.[a]Individual 3 also has a maternally inherited 17p13.2 deletion
[b]Clinical features as noted in MyGene2

of medical records (Figures 1 and S1; Table 1; Supplemental Note). The fourth individual, with a c.386C>G (p.Ser129Cys) variant, is presented with data drawn from MyGene2 (Table 1, Supplemental Note). The referring provider confirmed the submission, but the individual could not be enrolled in our study for detailed phenotypic evaluation. Comparison of all four affected individuals showed overlapping phenotypes consisting of severe complex ocular anomalies, dysmorphic craniofacial features, structural brain anomalies with severe neurological impairment, congenital heart defects, skeletal/spinal anomalies, genitourinary anomalies, feeding disorders with post-natal growth deficiency, structural gastroenterological anomalies, excess nuchal skin/cystic hygroma, hearing loss with recurrent otitis media, hip dysplasia, syndactyly, and contractures (Table 1). Height centiles were plotted for individuals 1 and 3 and showed normal length at birth with decreasing height centiles over time (Figure 1R); while a specific birth length was not available for individual 2, she was also reported to have a normal length at birth but fell to the 1st centile by age 2 months, similar to individual 1.

WDR37 is predicted to encode a 494-amino acid protein of unknown function (Figure S2). Literature review identified only two reports about this gene: one connecting WDR37 with osteoarthritis in rats and humans[11] and the other identifying it as one of several possible loci affecting renal function in humans.[12] Additional data collected via publicly available databases suggest a broad pattern of expression for Wdr37 in mice (BioGPS; Figure S3) with enrichment in ocular and brain tissues. Review of phenotype data for mice homozygous for a Wdr37 tm1a ("knockout first") allele (Wdr37tm1a(KOMP)Wtsi) from the International Mouse Phenotyping Consortium (IMPC) showed significant associations (p < .0001) with decreased body weight, decreased grip strength, and skeletal abnormalities of the spine, as well as a possible increase (p ≤ 0.05) in ocular (lens and corneal) anomalies, hearing defects, and changes in the size of the ulna, radius, and hindpaw. In addition, statistical analysis of the number of Wdr37 wild type, heterozygous, and homozygous pups from the IMPC indicates a significant decrease in the number of homozygous pups compared to expected Mendelian ratios (p < .001), suggesting decreased in utero

survival. This line has not been characterized to determine how the tm1a allele affects the function of Wdr37.

Protein sequence analysis predicts seven WD domains in the WDR37 C-terminal region from amino acid 154 to amino acid 493 (Figures 2A and S2) (Uniprot).[13] All the amino acids affected by the identified de novo variants are located upstream of the predicted WD domains and show high conservation among various species (Figure 2B). Analysis of wild-type WDR37 and its variants in silico using I-TASSER Suite and PyMOL predicted a seven-bladed propeller-like structure in the C-terminal region (corresponding to the seven WD-domains) with all four human variants located in the N-terminal region (Figure 2C); the missense variants are predicted to result in a conformational change affecting both the N- and C-terminal regions of the protein including the possible addition of an eighth propeller blade (Figure 2C). To further explore the functional role(s) of WDR37, we performed experiments in human cell culture and zebrafish (Supplemental Material and Methods).

Wild-type (WT) and mutant WDR37 (WDR37_Ser119Phe, WDR37_Thr125Ile, WDR37_Ser129Cys, and WDR37_Thr130Ile) FLAG-tagged expression constructs were generated and transfected into human lens epithelial cells (B-3 (ATCC CRL-11421)) to examine protein levels and cellular localization (Figure 3). Immunocytochemistry with anti-FLAG revealed a predominantly cytoplasmic staining for WT and all mutant proteins (Figures 3A–3J). These results were further verified using anti-FLAG western blotting of cytoplasmic- and nuclei-enriched fractions prepared from lens cells transfected with the above constructs. All mutant proteins demonstrated comparable levels and cellular distribution to wild-type WDR37 (Figures 3K and S4).

Analysis of the zebrafish genome identified a single ortholog for human WDR37, wdr37, located on chromosome 24. Analogous to humans, zebrafish wdr37 contains 14 exons with similar exon/intron structure and is also predicted to encode a 494-aa protein; the human and zebrafish proteins show 86% identity (Figure S2) and conservation for all positions affected in the presented individuals (Figure 2B). We performed expression studies of wdr37 using in situ hybridization. This analysis revealed robust and broad expression for wdr37 in zebrafish
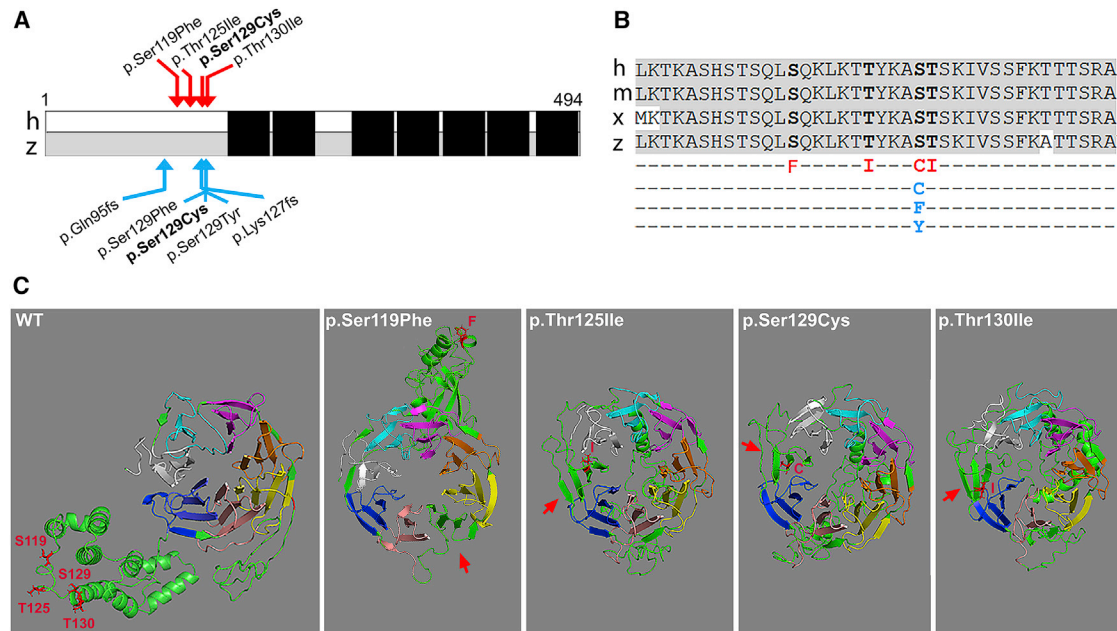
Figure 2. Characterization of WDR37 Variants

(A) Schematic of human (h) and zebrafish (z) WDR37/wdr37. Human variants are indicated above with red arrows and zebrafish variants are indicated below with blue arrows, WD domains are indicated with black boxes.

(B) Protein sequence alignment of the affected region. Sequence alignment shown for human (h; GenBank: NP_054742.2), mouse (m; GenBank: NP_001034477.1), *Xenopus* (x; GenBank: NP_001096465.1) and zebrafish (z; GenBank: NP_001161736.1) proteins. Human variants are indicated in red in line 5; zebrafish missense variants are shown in blue in lines 6, 7, and 8.

(C) Predicted WDR37 structure. Protein structure shown for WDR37 wild-type (WT) and mutant sequence, based on I-TASSER top predicted models; the top identified structural analog for the WT protein was RCSB Protein Data Bank assembly 5o9zl, a pre-catalytic human spliceosome primed for activation. Amino acids affected by human variants are indicated in red in WT structure; the red arrow indicates a predicted additional blade in mutant proteins. WT, wild-type; S, Ser; F, Phe; T, Thr; I, Ile; C, Cys; Y, Tyr.

embryos (Figure S3), indicating a possible role in development.

We first analyzed the effects of mutant *WDR37* on embryo development via injections of the mRNAs encoding for wild-type or mutant proteins (for the p.Thr125Ile and p.Ser129Cys variants) into fertilized zebrafish eggs at the 1- to 4-cells stage followed by observation of the developing embryos until 5 dpf (days post fertilization). Expression of exogenous human *WDR37* and encoded protein was confirmed via RT-PCR and western blot using 2-dpf embryos (Figure S4), but no visible effect on embryo development up to 5 dpf was observed.

We next utilized CRISPR-Cas9-mediated genome editing to generate novel alleles in zebrafish *wdr37*, both frameshift and missense. Three missense variants were identified in the offspring (F1) of mosaic founders (F0): c.386C>T (p.Ser129Phe), c.386C>G (p.Ser129Cys), and c. 386C>A (p.Ser129Tyr) (Figures 2A, 2B, and S1). All changes modify the Ser129 affected in individual 4 (with p.Ser129Cys being the exact replica of the human substitution) and were recovered in ~26%, 6%, and 2%, respectively, upon testing of 5- to 7-dpf progeny of various F0 mosaic parents. In addition, two frameshift alleles were isolated, c.377_396+4del p.Lys127Cysfs and c.282_291del p.Gln95Argfs, in ~10% and 14% of embryos produced by mosaic founders. The mosaic parents

were bred multiple times to generate additional progeny carrying the above variants, which were analyzed for their survival and phenotype. Similar to the results from injection of human mutant mRNA, no obvious phenotype was detected at 1–5 dpf. The most striking feature identified in F1 fish carrying the p.Ser129Phe, p.Ser129Cys, or p.Ser129Tyr heterozygous alleles was their larval lethality as no heterozygous animals were recovered after 1 month post fertilization (Figure 4A); in contrast, fish heterozygous for the c.377_396+4del and c.282_291del frameshift alleles were identified in 6% and 9% of their respective adult populations (at 2–3 months post fertilization). Statistical analysis confirmed significant differences between the proportion of embryos heterozygous for the p.Ser129Phe allele at either 5–7 or 9–14 dpf and at 17–19 or 30+ dpf (p < 0.0001), as well as the proportion of embryos heterozygous for the p.Ser129Cys alleles at either 5–7 or 9–14 dpf and at 30+ dpf (p < 0.0005) (Figure 4A). Similarly, no heterozygous larvae older than 30 dpf were detected for the p.Ser129Tyr allele (Figure 4A). Conversely, there was no significant difference between the proportion of heterozygous fish with frameshift *wdr37* variants at different stages with many animals surviving to adulthood. Careful observation under a stereomicroscope of mutant larvae carrying missense alleles at 6 dpf (n = 31) and 10 dpf (n = 33) did not identify any obvious defects
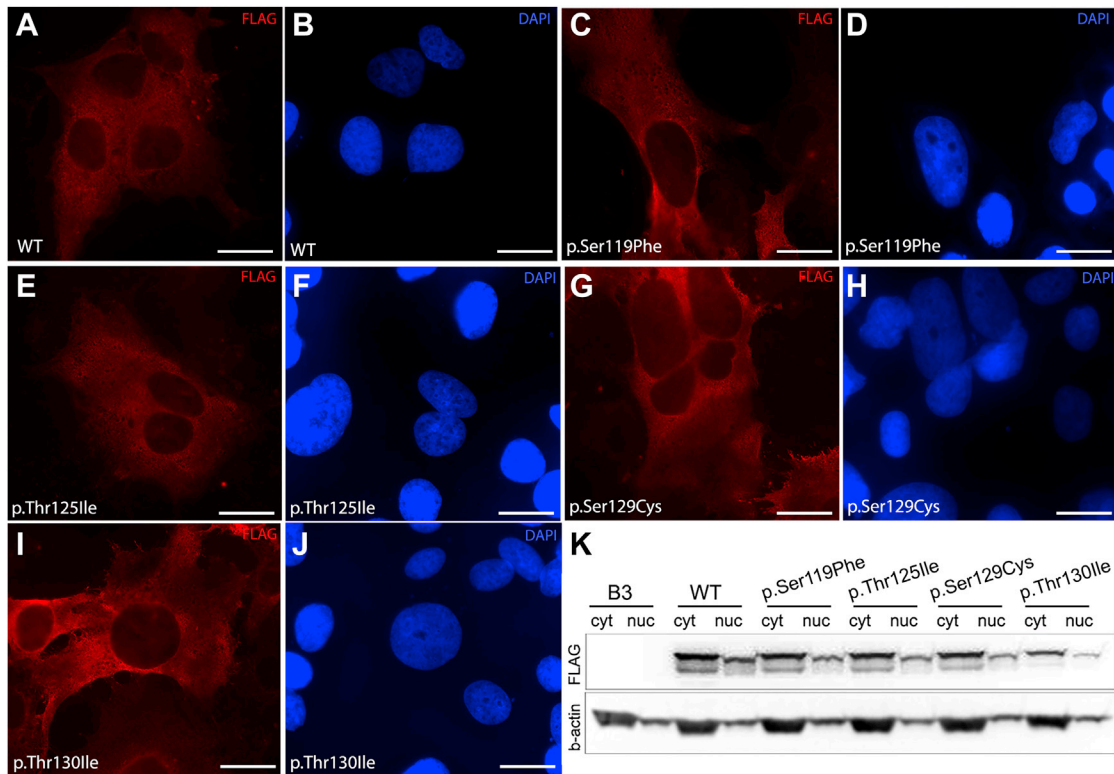
Figure 3. Protein Studies of Wild-Type and Mutant WDR37

(A–J) Immunocytochemistry demonstrating cellular localization of WT and mutant WDR37. Anti-FLAG staining (red) revealed predominantly cytoplasmic staining for wild type and all mutant proteins with missense variants. Specific variants are indicated in the lower left corner. DAPI staining in blue highlights the nucleus. Scale bar = 20 microns.

(K) Western blot analysis of cytoplasmic (cyt) and nuclear (nuc) fractions from human lens epithelial cells transfected with either WT or mutant WDR37 expression plasmids confirmed predominantly cytoplasmic presence with comparable patterns between mutant and wild type proteins. B3, untransfected B3 human lens epithelial cells; WT, wild-type.

that explain their early death; no coloboma, corneal anomalies, or consistent craniofacial abnormalities were observed. One common feature of fish carrying missense alleles was their poor growth prior to death (Figure 4B); measurements were undertaken for larvae heterozygous for p.Ser129Phe or p.Ser129Cys variants and confirmed a statistically significant decrease in overall body length (p < 0.01 and p < 0.05, correspondingly) as well as head size (significant for p.Ser129Phe only, p < 0.01) at 10 dpf, while body length and head size appeared normal at 6-dpf for both mutants (Figure 4C). The ratio of head to body length was calculated for both the missense mutants and wild-type embryos; comparison of these ratios did not identify any significant difference, indicating that the observed reduction in head size was not specific to the anterior structures but was proportionate to the overall decrease in body size. While additional studies are needed to determine the cause of the early lethality, overall, these data support a critical role for wdr37 in normal vertebrate development and pathogenicity of the missense alleles affecting the N-terminal region of WDR37/wdr37. The presence of a severe larval phenotype (poor growth, lethality) in heterozygous animals carrying missense but not frameshift variants suggests a

dominant-negative mechanism for the *WDR37/wdr37* missense alleles.

To identify possible pathways involved in *WDR37*-associated disease, RNA-seq was performed on RNA extracted from embryos heterozygous for the p.Ser129Phe variant and their wild-type siblings at 5 dpf. The expression levels of 145 zebrafish transcripts were affected, and human orthologs were identified for 92 of these (Figure 4D; Table S3). Analysis of these 92 transcripts using the Core Analysis function of Ingenuity Pathway Analysis identified upregulation of genes involved in cholesterol biosynthesis as the most significantly modified pathway (Figure 4E). Out of the 28 transcripts included in the Super Pathway of Cholesterol Synthesis, 9 were upregulated (activation z-score = 3 and p value 6.37E−16) (Figure 4F). The most affected cellular functions were steroid metabolism, which was significantly increased (z-score = 2.207), and accumulation of lipids, which was decreased (z-score = 1.747).

Based on the data presented here, heterozygous missense variants in *WDR37* in humans are causally associated with a multisystemic disorder characterized by poor growth and anomalies of the ocular, craniofacial, neurological, cardiovascular, genitourinary, skeletal, and gastrointestinal systems. Early lethality at less than 2 years of age occurred
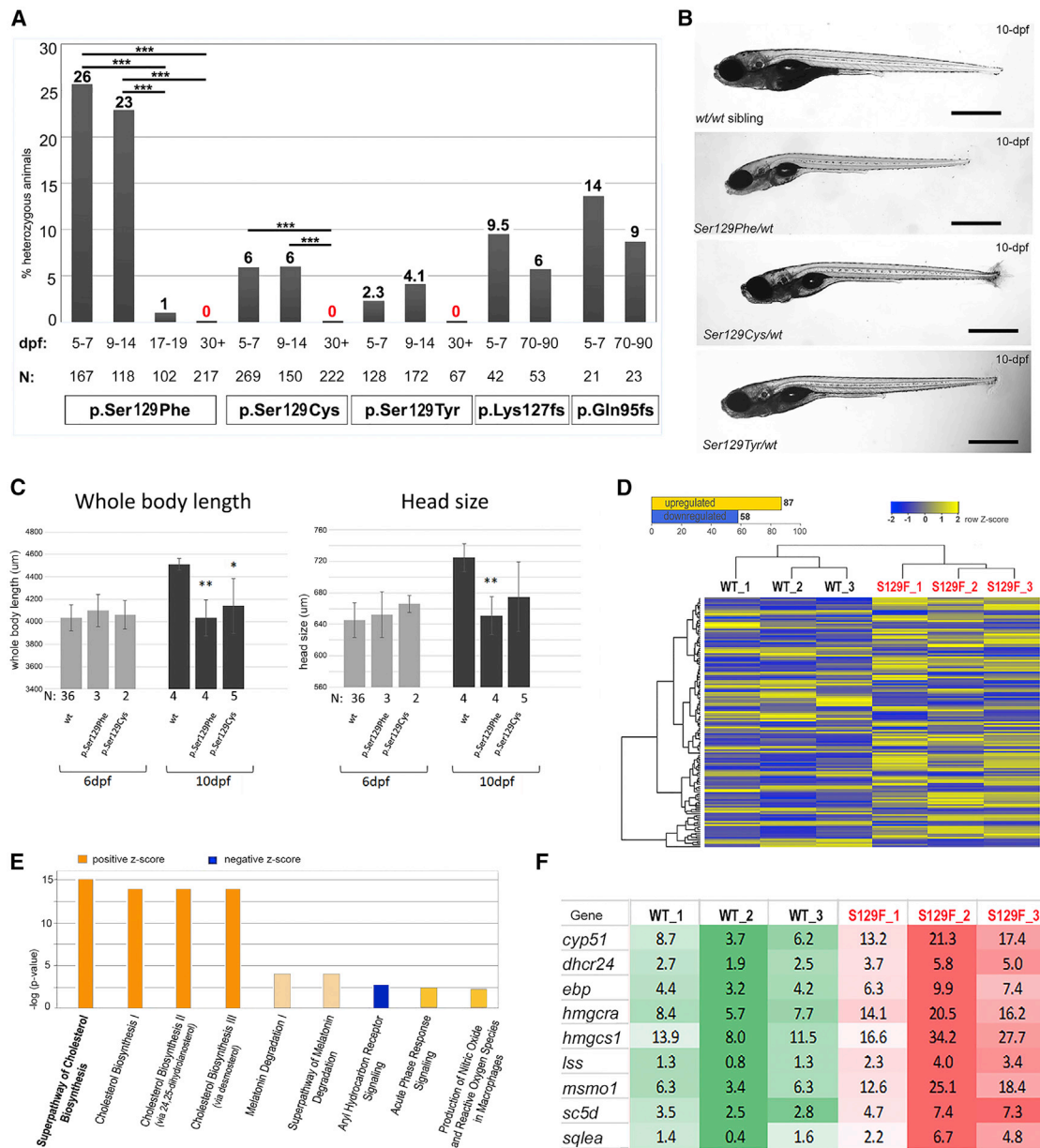
Figure 4. *wdr37* **Function in Zebrafish**

(A) Effect of *wdr37* variants on larval survival. Note that no larvae heterozygous for any missense allele were detected at 30+ dpf; conversely, similar percentages of animals carrying frameshift alleles were recovered at embryonic (5–7 dpf) and adult (70–90 dpf) stages. Black bars indicate the percentage of fish with heterozygous variants identified per stage, dpf corresponds to age (days post fertilization); N, total number of offspring genotyped; statistically significant differences indicated (***p < 0.0005).

(B) 10-dpf WT larvae and fish heterozygous for wdr37 p.Ser129Cys, p.Ser129Phe, p.Ser129Tyr variants are shown; fish carrying missense variants in general looked smaller and less viable; same magnification images are shown with scale bar = 775 microns.

(C) Total body length and head size data (in μm) for wild-type and mutant larvae at 6- and 10-dpf; N, total number of offspring measured; statistically significant differences indicated (**p < 0.01 and *p < 0.05).

(D) RNA-seq data analysis of 5-dpf *wdr37* heterozygous fish carrying the p.Ser129Phe allele in comparison to their wild-type siblings. 87 targets were upregulated and 58 were downregulated with p < 0.05 (see Table S1). Heatmap of the one-way hierarchical clustering using Z-score for normalized value (log2 based) that includes all 145 significantly changed transcripts is shown.

(E) Graphical representation of the top modified pathways identified through Ingenuity Pathway Analysis of transcripts altered in zebrafish heterozygous for the p.Ser129Phe variant shows cholesterol biosynthesis to be the top upregulated pathways.

(F) Heatmap of specific upregulated transcripts within the Super Pathway of Cholesterol Biosynthesis (Ingenuity Pathway Analysis). Out of the 28 transcripts included in the Super Pathway of Cholesterol Synthesis, 9 were upregulated (activation z-score = 3 and p value 6.37E−16) in heterozygous wdr37 p.Ser129Phe mutants in comparison to their wild-type siblings. The averaged FPKM (fragments per kilobase of transcript per million mapped reads) values are shown. S129F, p.Ser129Phe; WT, wild-type.

in one of four presented individuals. Zebrafish with CRISPR-Cas9-induced de novo missense variants similarly showed poor growth with shortened whole body length and proportionate small head evident by 10 dpf along with striking early lethality.

Two of the four individuals described here had clinical diagnoses of possible Peters-plus (PPS) or Walker-Warburg syndromes (WWS). The ocular phenotype in affected individuals is characterized by coloboma, lens anomalies, microcornea, and corneal opacity most consistent with Peters anomaly type 1, recently also described as kerato-irido-lenticular dysgenesis (KILD).[14] Each of the affected persons displayed multiple additional eye anomalies suggesting generalized ocular dysgenesis. Classic PPS is characterized by Peters anomaly along with other developmental ocular anomalies in some cases, short stature, brachydactyly, dysmorphic features, variable cleft lip/palate, cardiac, and genitourinary anomalies[8] and is caused by recessive pathogenic variants in glucosyltransferase B3GLCT.[3] Numerous individuals with similar, overlapping features that do not meet classic criteria are largely unexplained genetically.[1] WWS is a dystroglycanopathy characterized by both anterior and posterior segment ocular anomalies, muscular dystrophy, and severe structural brain anomalies with early death.[6] Recessive variants in 18 different genes have been identified in individuals with dystroglycanopathies, the majority of which are glycosyltransferases, with additional cases still unexplained.[7] Since both PPS and WWS are autosomal-recessive disorders while WDR37 syndrome is caused by de novo, dominantly expressed variants, accurate diagnosis is important for genetic counseling regarding recurrence risks.

The function of WDR37 is currently unknown. WD40 repeat (WD) domains represent a common protein interaction domain in humans, generally mediating interaction with other proteins, with more than 360 proteins identified that contain these regions.[15,16] Pathogenic variants in various WD domain-containing proteins have been linked to both dominant and recessive human ocular, neurological, skeletal, and genitourinary syndromes.[17,18] All of the variants reported here in WDR37 are upstream of the WD40 domains identified in Uniprot.[13] Similar dominant missense variants upstream of the identified WD domains have been identified in other WD proteins including WDR26 and TBL1XR1.[19] However, further structural modeling of one of these factors, WDR26, identified additional "imperfect" WD40 domains within the affected upstream region.[18]

RNA-seq data from mutant zebrafish suggest that WDR37 may play a role in the cholesterol biosynthesis pathway, with expression of dhcr24, sc5d, and ebp upregulated, among other transcripts. Comparison of the WDR37 phenotypes to known cholesterol biosynthesis disorders such as desmosterolosis (DHCR24 [MIM: 602398]), lathosterolosis (SC5D [MIM: 607330]), and MEND syndrome (EBP [MIM: 300960]) shows substantial overlap. Both groups are characterized by significant growth failure, structural brain defects, seizures, intellectual disability, microcephaly, ear and jaw anomalies, ophthalmological abnormalities (cataracts, microphthalmia, glaucoma, corneal clouding), defects of the cardiac, genitourinary, and skeletal systems, and early lethality.[20] Further work is needed to determine how WDR37 interacts with the cholesterol pathway.

Based on the data presented in this paper, pathogenic missense WDR37 variants appear to produce stable proteins while causing conformational changes disruptive to normal WDR37 activity. It is possible that WDR37 must dimerize to perform its function and that mutant WDR37 forms steady, yet functionally impaired, dimers with wild-type protein, thus exerting a dominant-negative effect. Further analysis is needed to determine the exact functional impact of the variants as well as the roles that WDR37/wdr37 plays in vertebrate development.

Accession Numbers

Supplemental Data

Acknowledgments

Declaration of Interests

The authors declare no competing interests

Web Resources

ArrayExpress, https://www.ebi.ac.uk/arrayexpress/
bioGPS, http://biogps.org/
gnomAD Browser, https://gnomad.broadinstitute.org/
IMPC, https://www.mousephenotype.org/
I-Tasser, https://zhanglab.ccmb.med.umich.edu/I-TASSER/

MyGene2, https://mygene2.org/MyGene2/
OMIM, https://omim.org/
PyMOL, https://pymol.org/
UniProt, https://www.uniprot.org/

References

1. Weh, E., Reis, L.M., Happ, H.C., Levin, A.V., Wheeler, P.G., David, K.L., Carney, E., Angle, B., Hauser, N., and Semina, E.V. (2014). Whole exome sequence analysis of Peters anomaly. Hum. Genet. *133*, 1497–1511.

2. Reis, L.M., and Semina, E.V. (2015). Conserved genetic pathways associated with microphthalmia, anophthalmia, and coloboma. Birth Defects Res. C Embryo Today *105*, 96–113.

3. Lesnik Oberstein, S.A., Kriek, M., White, S.J., Kalf, M.E., Szuhai, K., den Dunnen, J.T., Breuning, M.H., and Hennekam, R.C. (2006). Peters Plus syndrome is caused by mutations in B3GALTL, a putative glycosyltransferase. Am. J. Hum. Genet. *79*, 562–566.

4. Vissers, L.E., van Ravenswaaij, C.M., Admiraal, R., Hurst, J.A., de Vries, B.B., Janssen, I.M., van der Vliet, W.A., Huys, E.H., de Jong, P.J., Hamel, B.C., et al. (2004). Mutations in a new member of the chromodomain gene family cause CHARGE syndrome. Nat. Genet. *36*, 955–957.

5. Alrakaf, L., Al-Owain, M.A., Busehail, M., Alotaibi, M.A., Monies, D., Aldhalaan, H.M., Alhashem, A., Al-Hassnan, Z.N., Rahbeeni, Z.A., Murshedi, F.A., et al. (2018). Further delineation of Temtamy syndrome of corpus callosum and ocular abnormalities. Am. J. Med. Genet. A. *176*, 715–721.

6. Vajsar, J., and Schachter, H. (2006). Walker-Warburg syndrome. Orphanet J. Rare Dis. *1*, 29.

7. Bouchet-Séraphin, C., Vuillaumier-Barrot, S., and Seta, N. (2015). Dystroglycanopathies: About Numerous Genes Involved in Glycosylation of One Single Glycoprotein. J. Neuromuscul. Dis. *2*, 27–38.

8. Weh, E., Reis, L.M., Tyler, R.C., Bick, D., Rhead, W.J., Wallace, S., McGregor, T.L., Dills, S.K., Chao, M.C., Murray, J.C., and Semina, E.V. (2014). Novel B3GALTL mutations in classic Peters plus syndrome and lack of mutations in a large cohort of patients with similar phenotypes. Clin. Genet. *86*, 142–148.

9. Deml, B., Reis, L.M., Lemyre, E., Clark, R.D., Kariminejad, A., and Semina, E.V. (2016). Novel mutations in PAX6, OTX2 and NDP in anophthalmia, microphthalmia and coloboma. Eur. J. Hum. Genet. *24*, 535–541.

11. Korostyński, M., Małek, N., Piechota, M., and Starowicz, K. (2017). Blood Transcriptional Signatures for Disease Progression in a Rat Model of Osteoarthritis. Int. J. Genomics *2017*, 1746426.

12. Köttgen, A., Pattaro, C., Böger, C.A., Fuchsberger, C., Olden, M., Glazer, N.L., Parsa, A., Gao, X., Yang, Q., Smith, A.V., et al. (2010). New loci associated with kidney function and chronic kidney disease. Nat. Genet. *42*, 376–384.

13. The UniProt Consortium (2017). UniProt: the universal protein knowledgebase. Nucleic Acids Res. *45* (D1), D158–D169.

14. Nischal, K.K. (2015). Genetics of Congenital Corneal Opacification–Impact on Diagnosis and Treatment. Cornea *34* (*Suppl 10*), S24–S34.

15. Schapira, M., Tyers, M., Torrent, M., and Arrowsmith, C.H. (2017). WD40 repeat domain proteins: a novel target class? Nat. Rev. Drug Discov. *16*, 773–786.

16. Xu, C., and Min, J. (2011). Structure and function of WD40 domain proteins. Protein Cell *2*, 202–214.

17. Al-Rakan, M.A., Abothnain, M.D., Alrifai, M.T., and Alfadhel, M. (2018). Extending the ophthalmological phenotype of Galloway-Mowat syndrome with distinct retinal dysfunction: a report and review of ocular findings. BMC Ophthalmol. *18*, 147.

18. Skraban, C.M., Wells, C.F., Markose, P., Cho, M.T., Nesbitt, A.I., Au, P.Y.B., Begtrup, A., Bernat, J.A., Bird, L.M., Cao, K., et al.; Deciphering Developmental Disorders Study (2017). WDR26 Haploinsufficiency Causes a Recognizable Syndrome of Intellectual Disability, Seizures, Abnormal Gait, and Distinctive Facial Features. Am. J. Hum. Genet. *101*, 139–148.

19. Stenson, P.D., Mort, M., Ball, E.V., Shaw, K., Phillips, A., and Cooper, D.N. (2014). The Human Gene Mutation Database: building a comprehensive mutation repository for clinical and molecular genetics, diagnostic testing and personalized genomic medicine. Hum. Genet. *133*, 1–9.

20. Herman, G.E., and Kratz, L. (2012). Disorders of sterol synthesis: beyond Smith-Lemli-Opitz syndrome. Am. J. Med. Genet. C. Semin. Med. Genet. *160C*, 301–321.

Supplemental Data

De Novo Missense Variants in *WDR37*

Cause a Severe Multisystemic Syndrome

Linda M. Reis, Elena A. Sorokina, Samuel Thompson, Sanaa Muheisen, Milen Velinov, Carlos Zamora, Arthur S. Aylsworth, and Elena V. Semina

SUPPLEMENTAL NOTE: CASE REPORT

Individual 1 (Figure 1) is a 30-year-old White (Arabic/European descent) male. Karyotype and chromosomal microarray were normal. Clinical features below are from clinical exams and imaging.

Ocular: He had bilateral congenital glaucoma with optic nerve cupping requiring numerous surgeries, corneal opacity, microcornea (9 x 8mm OD and 6 x 7mm OS) and microphthalmia, and juvenile cataract. His right eye also had Peters anomaly (central corneal opacity and iridocorneal adhesions) and iris coloboma vs corectopia (keyhole pupil). His left eye had a totally opaque cornea with no view of the anterior chamber.

Craniofacial: He had significant microcephaly, arching eyebrows, thin upper lip, protruding upper and lower jaw with relative mid-face hypoplasia, large down-turned mouth, and simple and low set ears (Figure 1).

Neurological: He was non-verbal with very limited ambulation and seizures that began shortly after birth. Structural brain anomalies included Dandy-Walker variant (CSF collection in the posterior fossa which communicates with the fourth ventricle), mild enlargement of the ventricular system, delayed myelination and periventricular dysmyelination. Creatine Kinase (CK) level was normal at 17 years of age (130 with normal range of 0-200 U/L).

Cardiovascular: He had a ventricular septal defect, atrial septal defect, and patent ductus arteriosus.

Genitourinary: He had micropenis and cryptorchidism with incomplete puberty.

Growth: Length and weight were normal at birth at 21 inches (~53 cm; 75th-90th centile) and 8.5 pounds (3.9 kg; 50-75th centile), but by 1 year of age, his length and weight had fallen below the 3rd centile at 27 inches and 15 pounds 4 ounces (~69 cm and 6.9 kg, respectively). Growth hormone deficiency was diagnosed at 4 years of age and he was treated with growth hormone shots three times per week from 4 to 6 years of age with improved, but not normalized, growth trajectory. Treatment was discontinued at 6 years of age after a plateau in growth. At 14-15 years of age he went through abbreviated puberty with a growth spurt. At 17 years of age, his height, weight, and head circumference were all <3rd centile (128 cm, 30.2 kg, and 49 cm, respectively). Current adult height is just under 4 feet 6 inches (~136cm; <3rd; 50th centile for 9-year-old) and his weight fluctuates between 75-85 pounds (~34-38 kg; <3rd, 50th centile for 10 to 11-year-old). His head circumference was disproportionally small at 49.5 cm (50th centile for a 34-month-old) at 21 years of age.

Skeletal/spinal/limb: In addition to short stature, he had scoliosis, hip dysplasia with dislocation at 18 years of age; contractures of the interphalangeal and metacarpophalangeal joints, and pectus carinatum. He underwent bone lengthening procedures on both feet at 10 years of age to correct foot positioning.

Gastrointestinal: He had poor feeding from birth and progressive failure to thrive.

Other: Umbilical hernia.

Prenatal history: Fetal distress was noted prenatally, respiratory distress at birth.

Individual 2 (Figure 1) is a White (European descent) female who died at age 22 months. Clinical features below are from clinical exams, clinical imaging, and autopsy.

Ocular: Cloudy corneas were seen in the newborn nursery (NBN). On autopsy, the right eye showed Peters anomaly, microcornea (6x6 mm), uveal coloboma extending from iris to optic disc, areas of retinal dysplasia, and optic nerve hypoplasia. The left eye had an adherent corneal leukoma, microcornea (8x6 mm), aphakia, tiny uveal coloboma extending from iris to optic disc, inner retinal hypoplasia with focal dysplasia, microphthalmia, and focal optic nerve hypoplasia.

Craniofacial: She had significant microcephaly, the appearance of hypertelorism with lateral eyelid eversion, epicanthal folds, broad nasal bridge, ear anomalies (prominent antihelices, bilateral absent superior crus, hypoplastic tragi), smooth philtrum and upper lip vermilion, micrognathia, nuchal webbing, and multisutural craniosynostosis with predominant right lambdoid synostosis associated with marked flattening of the right side of the occiput.

Neurological: She was non-verbal, non-ambulatory, and hypotonic with seizures that began shortly after birth. Structural brain anomalies included Dandy-Walker spectrum malformation (dilated fourth ventricle and cerebellar hypoplasia with loss of inferior vermis), corpus callosum dysgenesis, pericallosal lipoma, abnormal gyration, cortical dysplasia, polygyria, decreased myelination of white matter, enlargement of the midbrain tectum, hypoplastic pons, abnormal morphology of the basal ganglia, and absence of olfactory tracts and bulbs. Hippocampi were small and incompletely inverted.

Brain MRI detailed review: Sagittal noncontrast T1 image at age 5 days (Fig. 1S) shows a prominent massa intermedia (asterisk), large midbrain tectum (large white arrow), and small pons. Corpus callosum is hypoplastic (thin white arrow) with a small rostrum and splenium. There is a bright pericallosal lipoma

and a Dandy-Walker variant with vermian hypoplasia (white arrowhead) and dilation of the fourth ventricle which communicates with the posterior fossa. Axial noncontrast T1 (Fig. 1T) demonstrates an abnormal gyral pattern with shallow sulci and broad gyri. The basal ganglia have an abnormal configuration with lack of visualization of the anterior limb of the internal capsule. On the axial T2 image (Fig. 1U), abnormal diffuse white matter hyperintensity is present in keeping with decreased myelination. Note the abnormally bright appearance of the posterior limb of the internal capsule (large black arrow) which should be myelinated (i.e. T2-dark) in a term infant and dysplastic, thickened cortex in the sylvian fissures (black arrowheads). Axial T2 image centered at the orbits (Fig. 1V) shows left microphthalmia without an identifiable lens. The contour of the right globe is also dysmorphic. The hippocampi are small and incompletely inverted and appear prominent.

Cardiovascular: At post, she had cardiomegaly with mesocardia and right atrial dilation, right ventricular hypertrophy, persistent large patent ductus arteriosis, ostium secundum atrial septal defect, two ventricular septal defects (one infracristal membranous, one muscular), tricuspid valve thickening with marked hooding of all three leaflets, bicuspid pulmonic valve, and marked dilation of the main pulmonary artery and its left and right branches.

Genitourinary: She had bilateral renal dysplasia with multiple small cortical cysts, bilateral hydronephrosis and hydroureter, bifid right ureter, a severely hypoplastic uterus, and tan, fibrotic-appearing thin ovaries

Growth: Length and weight were assessed as appropriate for gestational age (AGA) at her birth hospital, but by 2 months of age, her length and weight had fallen below the 3rd centile to 51 cm and 2.5 kg. Prior to her death, her weight was measured at 7.45 kg (50th centile for a 6.5-month-old) with her final length measured at 70.5 cm (50th centile for a 9-month-old). Her head circumference was disproportionately small. By 2 months of age, her head circumference was well below the 3rd centile and at 22 months of age, her head circumference was 50th centile for a 3-month-old. Length, weight, and head circumference were 70.5 cm, 5.86 kg, 40.2 cm, respectively, at autopsy (approximately 4.5, 4.7, and 4.8 standard deviations below the mean for chronologic age).

Skeletal/spinal/limb: In addition to short stature, she had mild thoraco-lumbar scoliosis, a sacral dimple with tethered cord, minimal right 2-3 toe syndactyly with second toe overlapping the third, appearance of mildly tapered fingers, and a bridged right palmar crease. Length was noted to be difficult to measure due to contractures.

Gastrointestinal: NG tube used from infancy due to poor intake; G-tube was placed at 8 months of age.

Other: She also had a bilobed right lung, normally positioned single spleen, pancreatic lipomatosis, diastasis recti, and possible hearing loss with recurrent otitis media.

Prenatal history: Maternal parvovirus infection. First trimester screening showed increased nuchal translucency (4.3 mm) consistent with cystic hygroma. Anatomy scan (17 weeks) found a probable dilated right pulmonary artery, probable duplicated right collecting system, echogenic bowel, and single umbilical artery. Fetal echocardiogram (19 weeks) showed bilateral fetal superior vena cava. Oligohydramnios in later pregnancy. Respiratory distress at birth.

Individual 3 (Figure 1) is an 8-year-old White (European descent) male. Chromosomal microarray identified a maternally-inherited deletion of 17p13.2 (4,327,373-4,541,334) of uncertain significance including the following OMIM genes: *SPNS3, SPNS2, MYBBP1A, GCT6, SMTNL2, ALOX15,* and *PELP1*. Clinical features below are from clinical exams and imaging. Karyotype and chromosomal microarray were normal.

Ocular: He had bilateral iris and chorioretinal colobomas extending to the optic disc with optic nerve dysplasia, horizontal nystagmus, and history of elevated intraocular pressure. Right eye also had retained pupillary membrane strands, retinal pigment contiguous dysplasia extending inferonasally to the peripheral chorioretinal coloboma, mild microcornea (10.5 mm), and anisometropic myopic astigmatism. Left eye also had Peters anomaly with central corneal leukoma, iris adhesions to the endothelium, and endothelial thinning, lens anterior capsule pigment plaque cataract extending into the cortex, and microcornea (9 mm)/microphthalmia (18.11 mm). Hypoplastic optic nerves were also noted on Brain MRI (described below).

Craniofacial: He had significant microcephaly, bitemporal narrowing, mild metopic prominence, small low-set and posteriorly rotated ears, square shaped ears, thin upper lip, thin and flattened mandible, high arched palate, short neck with excess nuchal skin posteriorly with webbing, epicanthal folds, upslanting palpebral fissures, ptosis, and a broad nasal bridge.

Neurological: He was non-verbal and non-ambulatory with seizures that began shortly after birth. Structural brain anomalies included Dandy-Walker variant (hypoplastic cerebellar hemispheres and inferior vermis with cystic dilatation of the fourth ventricle), hypoplastic corpus callosum with absence of the posterior cingulate gyrus, mild ventricular dilatation, delayed myelination, small sella, pituitary and infundibulum with absent posterior pituitary, hypoplastic optic nerves, optic tracts, and optic

chiasm. Gyration pattern was abnormal with broad gyri and shallow sulcations. Hippocampi were small and incompletely inverted.

Brain MRI detailed review: Sagittal noncontrast T1 image at age 11 days (Fig. 1W) shows that the corpus callosum is thinned but present (white arrows). Note enlarged massa intermedia, mildly prominent midbrain tectum, and a Dandy-Walker variant with hypoplastic cerebellar vermis. The optic chiasm and nerves appear atrophic (white arrowhead). The pituitary gland is small and the posterior pituitary bright spot is absent. Concurrent coronal T2 image (Fig. 1X) shows a simplified gyral pattern, diffuse white matter hyperintensity, and small and incompletely inverted hippocampi (black arrow). Follow-up sagittal noncontrast T1 at 11 months of life (Fig. 1Y) shows increased dilation of the posterior fossa and a relatively small brainstem. On the concurrent T2 image (Fig. 1Z) there is early myelination of the posterior limb of the internal capsule which appears dark (black arrowhead), significantly delayed for his age. Note extensive white matter volume loss with enlarged ventricles.

Cardiovascular: He had a persistent patent foramen ovale, patent ductus arteriosus, and prominent ventricular muscle bundle associated with tricuspid valve annulus.

Genitourinary: He had micropenis, cryptorchidism, and right hydronephrosis with recurrent urinary tract infections

Growth: At birth (39 3/7 weeks), his height, weight, and head circumference were all normal at 54.4 cm (90-95th centile), 3.582 kg (50th centile), and 35.5 cm (25th-50th centile). He had a normal human growth hormone level in infancy. His weight is normal with increasing centiles, but his height centile appears to be dropping with age. While accurate height is difficult to measure, from 3-6 years of age, his height measurements were generally between the 25-50th centile, while from 6-8 years of age, his height measurements were between the 3rd-25th centile. By 8 months of age, his head circumference had fallen below the 3rd centile. His head circumference was disproportionately small at 47.4 cm (50th centile for a 17-month-old) at 7.5 years of age.

Skeletal/spinal/limb: In addition to declining length centiles, he had hip dislocations and bilateral valgus deformities of the proximal femur, sacral dimple, hypoplastic proximal radii, bilateral 3-4 finger syndactyly, broad thumbs, clinodactyly, contractures of the 4th and 5th digits of the hand, bilateral sandal gap deformity, 2-4 toe syndactyly, and the appearance of a shortened metatarsal in the great toe.

Gastrointestinal: Malrotation with Ladd's bands obstructing the second part of the duodenum required surgical correction at 1 month of age (Ladd's procedure and inversion appendectomy). He also had a

feeding disorder with feeding intolerance and severe gastroesophageal reflux disease requiring g-tube and fundoplication at 2 months of age. He was noted to have a small stomach with large left lobe of the liver. Feeding intolerance continued and he remains entirely g-tube fed.

Other: Hearing loss with history of recurrent otitis media and four sets of PE tubes, mild hypothyroidism (familial), leg length discrepancy, and poor immune function with hypogammaglobulinemia (also present in mother and brother).

Prenatal history: Low fetal heart rate, breech presentation, very small and short umbilical cord and decreased amniotic fluid volume noted at delivery. Respiratory distress required admission to the Neonatal Intensive Care Unit shortly after birth.

Individual 4 has limited information available as summarized in MyGene2 (https://mygene2.org); all other features are unknown.

Ocular: Coloboma

Craniofacial: Hypertelorism, long eyelashes, prominent forehead, downturned corners of the mouth, microcephaly, prominent nasal bridge, low-set ears.

Neurological: Global developmental delay, seizures, cerebellar hypoplasia.

Cardiovascular: Abnormal heart morphology.

Genitourinary: Not noted.

Skeletal/spinal/limb: Growth delay, single transverse palmar crease, tapered fingers, joint laxity.

Gastrointestinal: Not noted.

Other: Not noted.
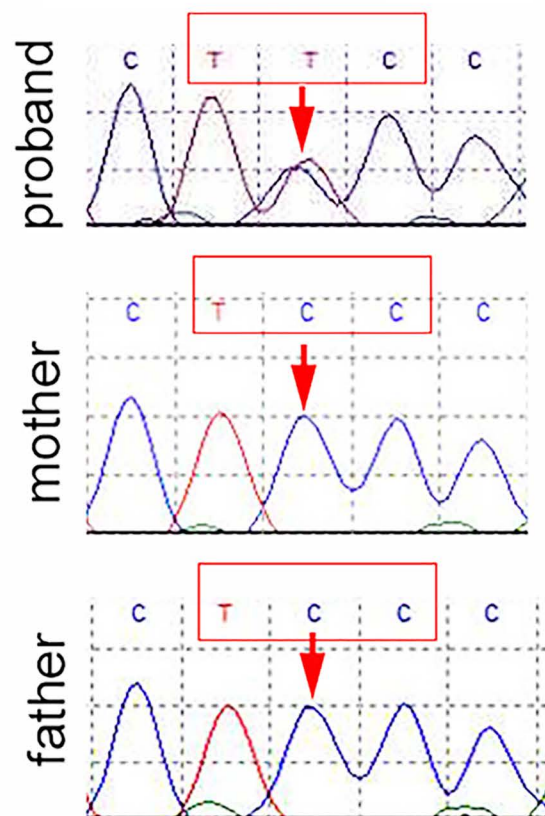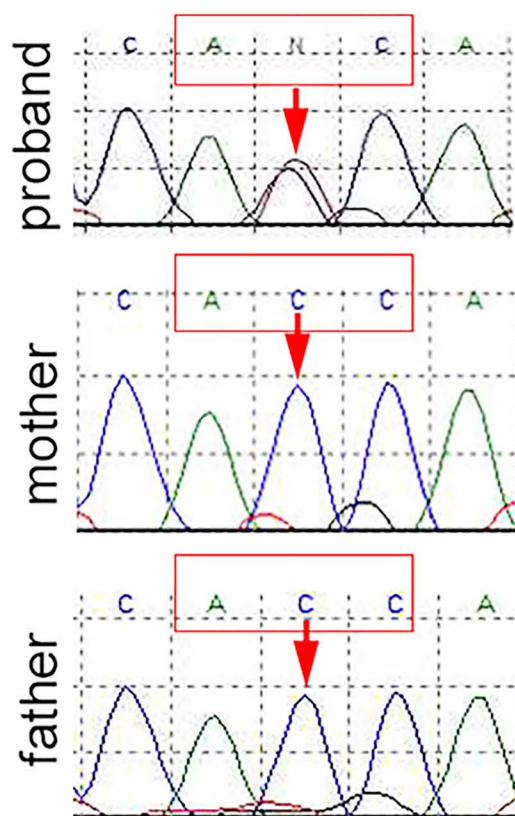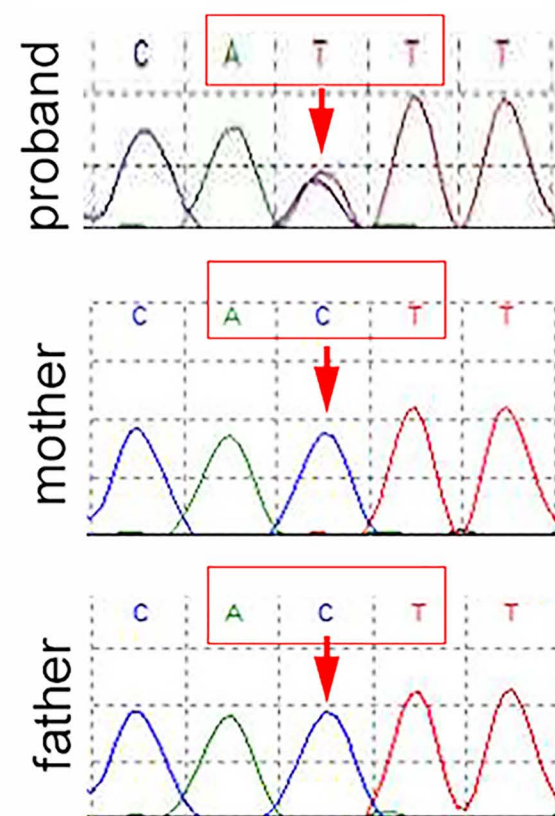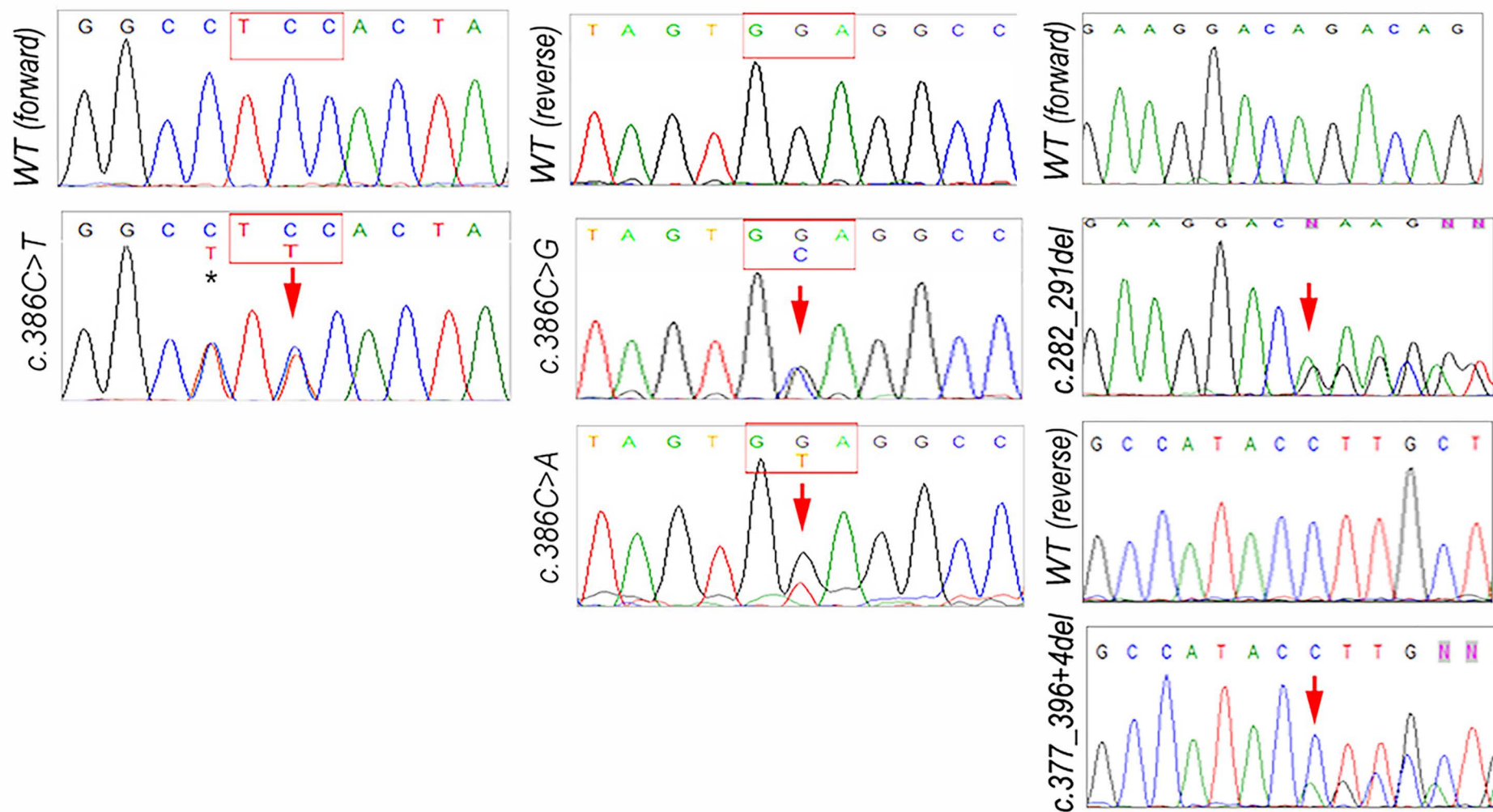
Prenatal history: Not noted.

Figure S1: Sequencing data for *WDR37/wdr37* variants. A. *WDR37* sequencing data for Patients 1-3 and their parents. Sequence traces for each trio show heterozygous variant in the affected patient and normal sequence in parents. Red box indicates the affected codon. **B**. *wdr37* sequencing data for zebrafish mutants. Sequencing traces show genotyping results for each mutation (indicated with red arrow) with wild type region above. Forward sequences are shown for the c.386C>T and c.282_291del variants; reverse sequences are provided for the c.386C>G, c.386C>A and c.377_396+4del alleles. The * marks a second silent variant in one of the lines, c.384C>T p.Ala128Ala.

```
                    1                                                                            92
Human      MPTESASCSTARQTKQKRKSHSLSIRRTNSSEQERTGLPRDMLEGQDSKLPSSVRSTLLELFGQIEREFENLYIENLELRREIDTLNERLAA
Mouse      MPTESGSCSTARQAKQKRKSHSLSIRRTNSSEQERTGLPREMLEGQDSKLPSSVRSTLLELFGQIEREFENLYIENLELRREIDTLNERLAG
Xenopus    MPTESGSWAAARQTKQKRKSHSLSIKRTNSSEQDRPGLQREMLEGQDSKLPSSVRNTLLELFGQIEREFENLYLENLELRREIDTLNDRLAV
Zebrafish  MPVESGNSAAARQVKQKRKSHSLSIRRTNSTEQDRTGMQRDMLEGQDSKLPMALRSNLLDLFGQIEREFENLYIENLELRREIESLNERLSG

                    93                                                                           184
Human      EGQAIDGAELSKGQLKTKASHSTSQLSQKLKTTYKASTSKIVSSFKTTTSRAACQLVKEYIGHRDGIWDVSVAKTQPVVLGTASADHTALLW
Mouse      EGQAIDGAELSKGQLKTKASHSTSQLSQKLKTTYKASTSKIVSSFKTTTSRAICQLVKEYIGHRDGIWDVSVTRTQPIVLGTASADHTALLW
Xenopus    EGQAIDGAELSKGQMKTKASHSTSQLSQKLKTTYKASTSKIVSSFKTTTSRAICQLVKDYVGHRDGLWDVSVTRTQPVVLGTASADHTALLW
Zebrafish  EGQTVEGGDLSKGALKTKASHSTSQLSQKLKTTYKASTSKIVSSFKATTSRAVCQLVKEYVGHRDGIWDLAVTRVQPLVLGTASADHCSMLW
           ----------------------------------------F----I--CI-----------------------------------------

                    185                                                                          274
Human      SIETGKCLVKYAGHVGSVNSIKFHPSEQLALTASGDQTAHIWRYAVQLPTPQPVADTS--ISGEDEVECSDKDEPDLDGDVSSDCPTIRVPL
Mouse      SIETGKCLVKYAGHVGSVNSIKFHPSEQLALTASGDQTAHIWRYVVQLPTPQPVADTSQQISGEDEIECSDKDEPDIDGDVSSDCPTVRVPL
Xenopus    SIETGKCLIKYVGHAGSVNSIKFHPTEQIALTASGDQTAHIWRYMVQLPTPQPTADTS--ISGEEEVDFSDKDENDGDDASSDCPTVRVPL
Zebrafish  SIETGKCLLKYAGHAGSVNSIKFHPTEQMALTASGDQTAHIWRYMVQLPLPQPPADIS--ASLDDVDFSDKDEADGDADGPNECPTIRVAT

                    275                                                                          366
Human      TSLKSHQGVVIASDWLVGGKQAVTASWDRTANLYDVETSELVHSLTGHDQELTHCCTHPTQRLVVTSSRDTTFRLWDFRDPSIHSVNVFQGH
Mouse      TSLKSHQGVVIAADWLVGGKQVVTASWDRTANLYDVETSELVHSLTGHDQELTHCCTHPTQRLVVTSSRDTTFRLWDFRDPSIHSVNVFQGH
Xenopus    TALKSHQGVVIAADWLVGGKQAVTASWDRTANLYDVETSELVHSLTGHDQELTHCCTHPTQRLVVTSSRDTTFRLWDFRDPSIHSVNVFQGH
Zebrafish  TTLKSHQGVVIAADWLVGGKQVVTASWDRAANLYDVETSELVHTLTGHDQELTHCCTHPTQRLVVTSSRDTTFRLWDFRDPSIHSVNVFQGH

                    367                                                                          458
Human      TDTVTSAVFTVGDNVVSGSDDRTVKVWDLKNMRSPIATIRTDSAINRINVCVGQKIIALPHDNRQVRLFDMSGVRLARLPRSSRQGHRRMVC
Mouse      TDTVTSAVFTVGDNVVSGSDDRTVKVWDLKNMRSPIATIRTDSAINRINVCVGQKIIALPHDNRQVRLFDMSGVRLARLPRSSRQGHRRMVC
Xenopus    TDTVTSAVFTVGDNVVSGSDDRTVKVWDLKNMRSPIATIRTDSAINRISVSVGQKIIALPHDNRQVRLFDMSGVRLARLPRSNRQGHRRMVC
Zebrafish  TDTVTSAVFTVGDNVVSGSDDRTVKVWDLKNMRSPIATIRTDSAVNRISVSANQRIIALPHDNRQVRLFDMNGVRLARLPRSNRQGHRRMVC

                    459                                   494
Human      CSAWSEDHPVCNLFTCGFDRQAIGWNINIPALLQEK
Mouse      CSAWSEDHPICNLFTCGFDRQAIGWNINIPALLQEK
Xenopus    CCAWSEDHPTCNLFTCGFDRQAIGWNINIPALLQEK
Zebrafish  CSAWNEENQACNLFTCGFDRQAIGWNINIPALLQEK
```

Figure S2: WDR37 full sequence alignment. Full WDR37 sequence shown for human (NP_054742.2), mouse (NP_001034477.1), xenopus (NP_001096465.1) and zebrafish (NP_001161736.1). Residues conserved in three or more species are shaded in gray, human variants are indicated in red below, and WD domains are indicated as green boxes below.

A

Dataset: GeneAtlas MOE430, gcrma
Probeset: 1434077_at
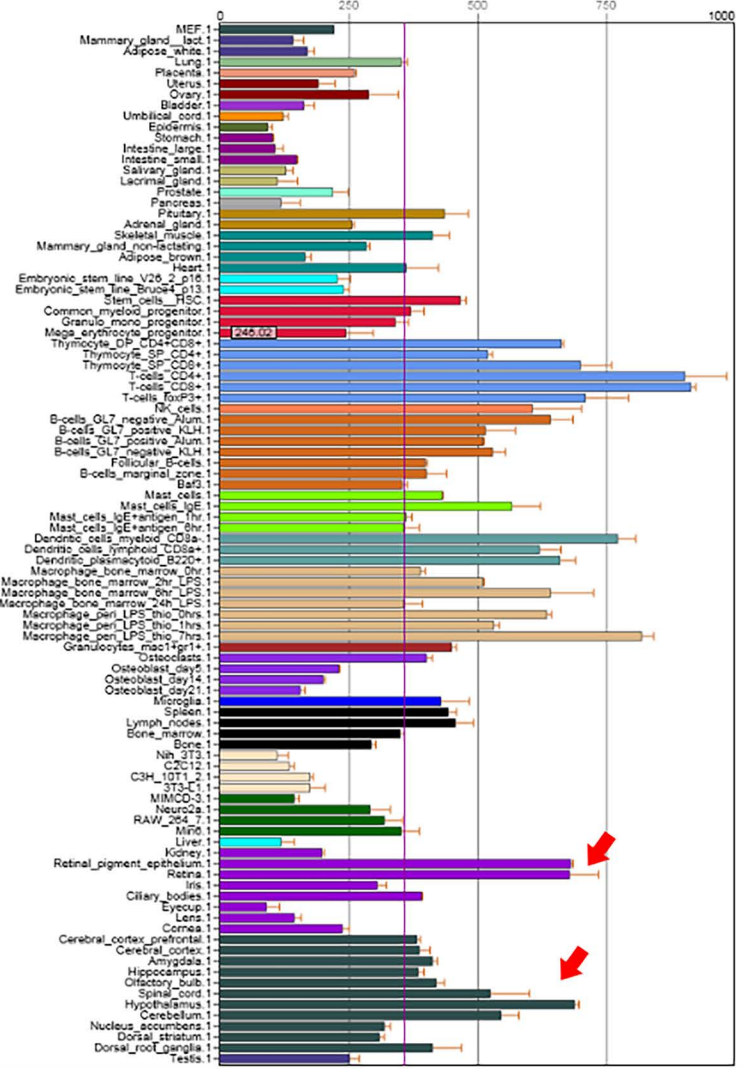
Dataset: GeneAtlas MOE430, gcrma
Probeset: 1434076_at
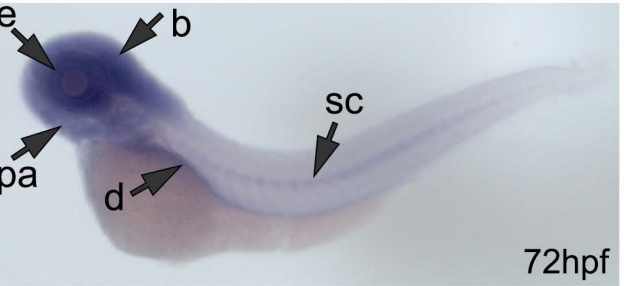
B
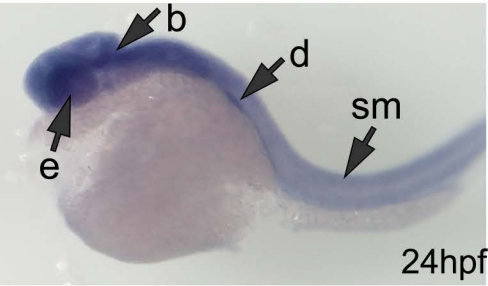
20hpf — t, e

24hpf — b, e, d, sm

72hpf — e, b, pa, d, sc
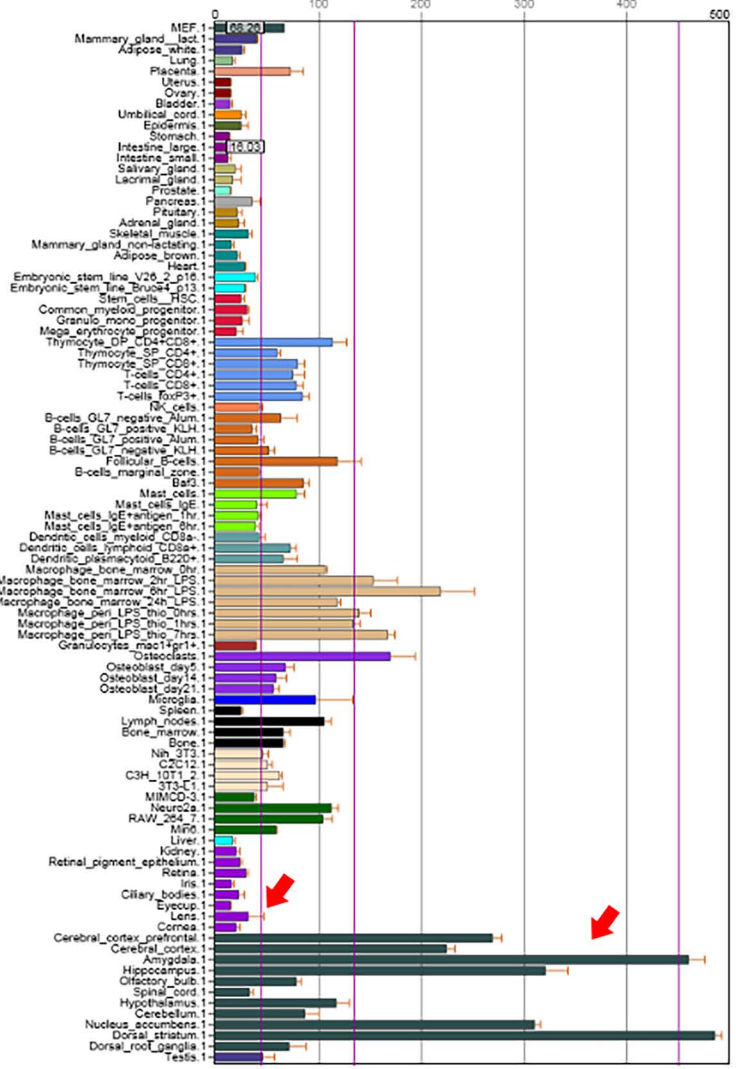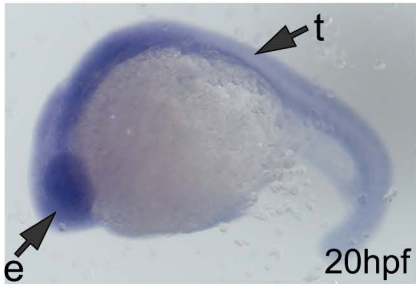
Figure S3: Expression of *Wdr37/wdr37* in different species. A. Relative expression of *Wdr37* in various mouse tissues. Review of expression data from BioGPS.org for *Wdr37* (Probesets 1434077 and 1434076). Red arrows indicate enriched eye and brain expression. **B**. *wdr37* expression in zebrafish embryos. Note broad expression of *wdr37* in zebrafish embryos at 20, 24 and 72 hours post fertilization (hpf); e- eye, b- brain, d- digestive system, pa- pharyngeal arches, sm- skeletal muscles, sc- spinal cord, t-trunk.

A
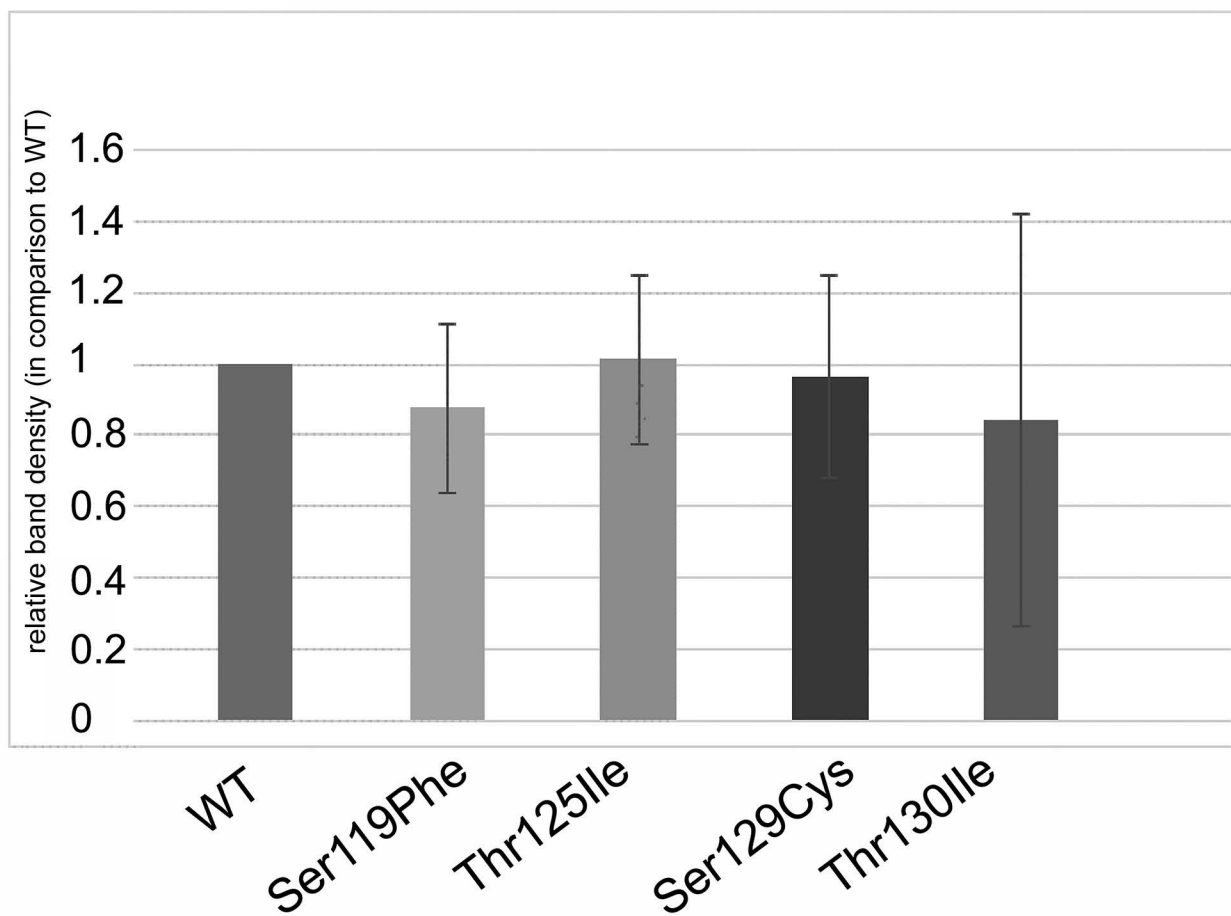
B

2-dpf zebrafish embryos
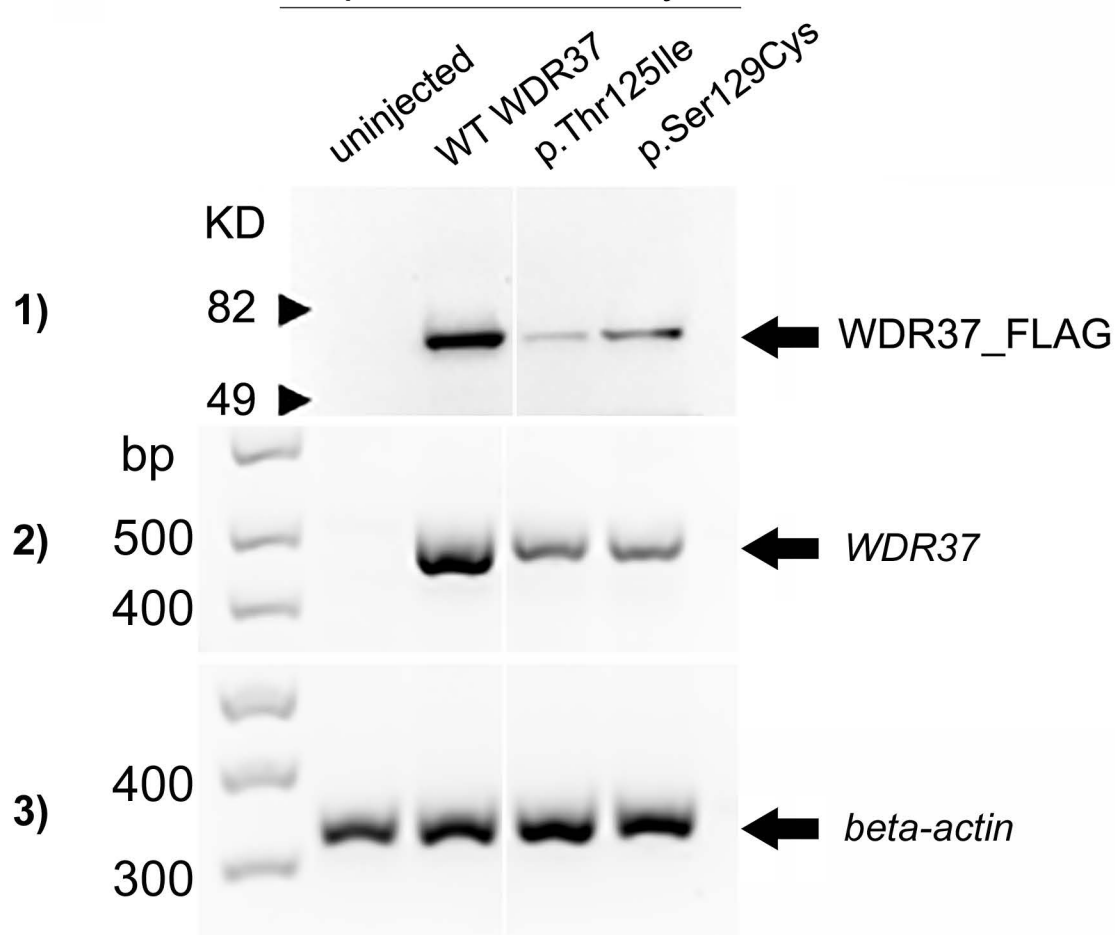
Figure S4. Western blot and RT-PCR data. A. Results of quantitative analysis of Western blot (n=4) data for WDR37 wild-type and variant proteins. No statistically significant difference was observed based on t-test (between each of the variants and wild-type). **B**. Western blot and RT-PCR data showing the presence of: 1) FLAG-tagged human WDR37 wild-type (WT) and mutant (p.Ser129Cys and p.Thr125Ile) and 2) human WT and mutant transcripts in 2-dpf embryos injected with mRNA encoding for the corresponding proteins but not in uninjected control embryos; 3) zebrafish *beta-actin* transcript in all samples.

Table S1. Exome data coverage statistics for presented cases.

Data/Sample	Agilent Capture Kit	Total yield (bp)	Average read length (bp)	Initial mappable reads (mapped to human genome)	% Initial mappable reads (out of total reads)	Non-redundant reads (de-duplicated by Picard tools)	% Non-redundant reads (out of initial mappable reads)	% Coverage of target regions (more than 10X)	Mean depth of target regions (X)
Individual 1	SureSelect_V4	3768468166	101	37182092	99.7	36342818	97.7	94.9	49.4
Mother (Individual 1)	SureSelect_V4	3255337060	101	32130068	99.7	31031546	96.6	94.5	43.6
Father (Individual 1)	SureSelect_V4	3335517324	101	32914712	99.7	31871923	96.8	94.5	44.6
Individual 2	SureSelect_V4	4069822068	101	40108676	99.5	39001530	97.2	96.2	53.8

Table S1. Exome data coverage statistics for presented cases. Statistical data for Individual 1 (and parents) and Individual 2 is summarized.

Table S2. Variants of uncertain significance in *WDR37*

Individual	Phenotype	DNA change	Protein change	gnomAD frequency	In silico predictions	Family analysis
Individual 1	See manuscript	c.1255G>A	p.Gly419Ser	13/277096	Damaging by 2/5 (MT, F)	Inherited from an unaffected parent
Individual 5	Unilateral cataract with iridolenticular adhesions, heart defect, MRSA meningitis	c.770C>A	p.Pro257His	1/250886	Damaging by 2/5 (MT, F)	Inherited from an unaffected parent
Individual 6	Glaucoma and iris hypoplasia	c.1330C>T	p.Arg444Trp	1/251398	Damaging by 5/5 (S, PP2, MT, MA, F)	Not present in 5 affected family members

S: SIFT, PP2: PolyPhen2, MT: MutationTaster, MA: MutationAssessor, and F: FATHMM MKL

Table S2. Variants of uncertain significance in *WDR37*. Additional rare variants in *WDR37* and their features are presented. Based upon testing of family members, general population data, and in silico predictions, all are considered likely benign.

Table S3. Summary of 145 significantly changed transcripts. Zebrafish gene ID, transcript ID, ZFIN number and gene symbol, the gene name and OMIM# of an identified human ortholog, when available, along with the fold change and raw p-value are presented (sorted in order from most downregulated to most upregulated).

SUPPLEMENTAL MATERIALS AND METHODS

Human sequencing

This human study was approved by the Institutional Review Board of the Children's Hospital of Wisconsin with written informed consent obtained for participation and publication for every participant. Genomic DNA from Individual 1 and his parents and Individual 2 was submitted for exome sequencing as previously reported to Axeq (now Macrogen)[1]; prior analysis excluded pathogenic variants in *B3GLCT* and other known ocular genes[2]. Trio analysis was performed using SNP and Variation Suite (Golden Helix) and variants of interest were annotated using gnomAD and dbNSFP tracks for frequency in the general population and in silico predictions (SIFT, Polyphen2, MutationTaster, MutationAssessor, and FATHMM MKL), respectively. Individuals 3 and 4 were identified through the matchmaker website MyGene2[3] and Individual 3 was subsequently enrolled in the study. Sanger sequencing of *WDR37* exon 5 was undertaken in Individuals 1-3 and all parents to confirm the variants of interest and determine co-segregation using the following primers: TCCTGTGCAAGACACAAGAC (F) and TACAAGCATGAGCCACCATG (R).

Growth data graphing

Height centiles for Individuals 1 and 3 at each time point were determined using the CDC Growth Calculator for 0 to 36 months or 2 to 20 years, as appropriate, at https://peditools.org. Centiles were graphed by age (years) using Excel for Individuals 1 and 3 only since a specific birth length measurement was not available for Individual 2.

Analysis of IMPC mouse data

Phenotypes for *Wdr37*[tm1a(KOMP)Wtsi] mice were obtained from the International Mouse Phenotyping Consortium (IMPC) website, http://www.mousephenotype.org/data/genes/MGI:1920393#section-associations. We performed a Chi-square goodness-of-fit test comparing the IMPC reported numbers of wild-type, heterozygous, and homozygous pups with the *Wdr37*[tm1a(KOMP)Wtsi] allele to expected mendelian ratios for a compound heterozygous cross. Data for the numbers of pups was obtained at: http://www.mousephenotype.org/data/charts?accession=MGI:1920393&allele_accession_id=MGI:4452651&zygosity=homozygote&parameter_stable_id=IMPC_VIA_001_001&pipeline_stable_id=MGP_001.

Protein alignments and modeling.

In silico analysis of wild-type and mutant WDR37 was undertaken. Modeling of the WDR37 wild-type (NP_054742.2) and mutant structures was completed using I-TASSER[4] (https://zhanglab.ccmb.med.umich.edu). The top model for each sequence was selected; for the wild-type protein, the top structural analog used for modeling was RCSB Protein Data Bank assembly 5o9zl, a pre-catalytic human spliceosome primed for activation (https://www.rcsb.org/structure/5o9z). The top models were uploaded into PyMOL Molecular Graphics System, Version 2.2 (Schrödinger, LLC; https://pymol.org/2/) for labelling of specific amino acids and coloring of domains.

Site-directed mutagenesis.

The plasmid pEZ-M14 encoding full-length human WDR37 in fusion with 3xFLAG tag (GeneCopoeia, EX-A3878-M14) served as a template for site-directed mutagenesis. The QuikChange XL Site-Directed Mutagenesis Kit (Agilent Technologies) was used to introduce 4 different variants into this gene. The following mutagenesis primers were utilized: for the c.356C>T variant 5'-cttcagtttctggaagagctggctggtgctg and 5'- cagcaccagccagctcttccagaaactgaag; for the c.374C>T variant 5'-tggtggaagccttgtaaatggtcttcagtttctgg and 5'- cagaaactgaagaccatttacaaggcttccacca; for the c.386C>G variant 5'- aatcttgctggtgcaagccttgtaagtggtcttc and 5'- gaagaccacttacaaggcttgcaccagcaagatt; and for the c.389C>T variant 5'- tggagacaatcttgctgatggaagccttgtaagtg and 5'- cacttacaaggcttccatcagcaagattgtctcca. Primers were designed using the QuikChange Primer Design Program (Agilent Technologies). All variants were verified by Sanger sequencing.

Cell culture and transfection.

The B3 human lens epithelial cell line (ATCC® CRL-11421™) was maintained in Eagle's Minimum Essential Medium supplemented with 20% fetal bovine serum. Approximately 10^7 cells were transfected with 7.5μg of DNA encoding WDR37 variants and Lipofectamine 2000 reagent (Invitrogen). Experiments were performed with wild-type *WDR37* and mutant constructs with each of the identified human variants: WDR37_S119F (p.Ser119Phe), WDR37_T125I (p.Thr125Ile), WDR37_S129C (p.Ser129Cys), and WDR37_T130I (p.Thr130Ile). On the day following transfection, cells were transferred to 2 plates and after an additional 24 hours either used for immunofluorescence or harvested for Western blot analysis.

Immunofluorescence staining

24 hours post-transfection cells were sub-cultured into a 35mm glass bottom dish (Cellvis). After an additional 24 hours, cells were rinsed with PBS (Phosphate Buffered Saline) buffer and fixed with 4%

paraformaldehyde in PBS for 15 minutes at room temperature, permeabilized with 0.25% TritonX-100 and blocked with 3% normal donkey serum in PBS. Plates were incubated with 1:500 dilution of anti-FLAG M2 mouse monoclonal antibody (Cell Signaling Technology) in 3% normal donkey serum overnight followed by donkey anti-mouse IgG secondary antibody conjugated with AlexaFluor[tm] 568 (Invitrogen). All washes between these steps were done with 1xPBS. Cells were overlaid with DAPI-containing Fluoromount-G (eBioscience) mounting media and imaged with All-in-One Fluorescence Microscope (Keyence).

Protein extraction and Western blot

Transfected cells were fractionated with the Nuclear Extraction Kit (Millipore Sigma) which sequentially extracts cytoplasmic and nuclear proteins by incubation with hypotonic buffer followed by centrifugation and extraction of the remaining crude nuclear pellet with a high-salt buffer according to the manufacturer's protocol. 22 µl out of the total 500 µl of each cytoplasmic fraction and 15 µl out of the total 45 µl of each nuclear fraction were loaded for every transfected variant and control untransfected cells onto an 18-well 4-15% Criterion Precast Gel (Bio-Rad). Resolved proteins were transferred into Immobilon-P transfer membrane (Millipore) and probed with anti-FLAG M2 mouse monoclonal antibody (Sigma) as a primary antibody and goat-anti mouse IgG1 as a secondary antibody, HRP conjugate (Invitrogen). The control β-Actin Antibody (Santa Cruz Biotechnology, sc-81178) in dilution 1:500 was used as a cytoplasmic fraction marker. After exposure to the SuperSignal West Pico chemiluminescent substrate ESL reagent (Thermo Scientific) the signal was detected with the iBrightFL1000 imager (Invitrogen). Quantification of Western blot (n=4) results was performed using ImageJ (https://imagej.nih.gov/ij/) and relative (to WT) band density was calculated for each mutant; the t-test was used to compare the mean value for each WDR37 variant to wild-type.

Analysis in zebrafish

To further explore the role of wild-type and mutant *WDR37/wdr37,* additional experiments were designed and carried out in zebrafish. All zebrafish experiments were approved by the Medical College of Wisconsin Institutional Animal Care and Use Committee (IACUC).

In situ hybridization

in situ hybridization was performed using an antisense *wdr37* probe generated as follows: a 747-bp fragment specific for the zebrafish *wdr37* transcript was first generated using the following primers, 5'-

GCGTCTGTCAGGAGAAGGAC and 5'-AGACGCTGAGTCGGATGAGT and inserted into a pCRII-TOPO vector. This construct was extracted, purified and precipitated after being linearized with EcoRV and the antisense probe was generated using DIG RNA Labeling mix (Roche Diagnostics) and SP6 RNA polymerase (Roche Diagnostics). The probe was precipitated then purified using Micro Bio-Spin Columns (Bio-Rad). In situ hybridization was then performed with this probe following previously described protocols[5].

mRNA synthesis and injection

Capped and polyadenylated human *WDR37* mRNA was synthesized using mMESSAGE mMACHINE® T7 Ultra Kit (Ambion) according to the manufacturer protocol. The Ringer solution containing 300ng of mRNA encoding WT or either one of the c.386C>G and c.374C>T *WDR37* mutants was injected into single cell embryos (n=50-100) using the NanojectII injector (Drummond Scientific). In order to verify human *WDR37/*WDR37 expression, equal numbers of injected or noninjected embryos were collected at 2 dpf for RT-PCR (n=5 for each group) and Western Blot analysis (n=20 for each group). The RNA was extracted using Direct-zol RNA MiniPrep kit (Zymo Research). The cDNA was synthesized with SuperScript First-Strand Synthesis System for RT-PCR (Invitrogen) and amplified with either human-specific primers for the *WDR37* transcript (5'- GAGAGGACGGGACTGCCA and 5'- GGCCTGCGTACTTGACTAGG; product size is 493bp) or primers for the zebrafish *beta-actin* transcript (5'- GAGAAGATCTGGCATCACAC and 5'- ATCAGGTAGTCTGTCAGGTC; product size is 323bp). Embryos collected for protein studies were deyolked in 1/2 Ginzburg Fish Ringer buffer and homogenized in 60µl of RIPA buffer in the presence of protease inhibitor cocktail (Sigma). Recombinant protein expression was verified by Western Blot as described above. The membrane was probed with mouse monoclonal anti-FLAG M2 antibody (Sigma). After incubation with HRP-conjugated secondary antibody the signal was detected with SuperSignal West Pico Chemiluminescent Substrate (Thermo Scientific).

Producing of mutant zebrafish lines and fish observations

The pCMV-BE-zCas9 vector (Addgene, Plasmid #101739) was used to synthesize the modified version of Cas9[6]. The vector was linearized with BamHI and mRNA was produced using the mMESSAGE mMACHINE® T7 Ultra Kit (Ambion). To create precise base conversions in zebrafish *wdr37*, gRNA (5'- GGCCTCCACTAGCAAGGTA) targeting the enzyme to this sequence in *wdr37* exon5 was designed. The DNA fragment encoding gRNA was cloned into the BsaI site of the DR274 vector (Addgene, Plasmid #42250)[7]. The vector was linearized by a DraI restriction enzyme and gRNA was expressed using the

MEGAshortscript T7 Transcription Kit (Thermo Fisher Scientific) following the manufacturer's protocol. Guide RNA was purified with the RNA Clean&Concentrator^{tm}-5 kit (Zymo Research).

Approximately 9 nl of the mixture containing 600pg of BEcas9 mRNA and 25pg of gRNA in Ringer buffer was injected into each single-cell stage zebrafish embryo using the NanojectII injector (Drummond Scientific). The F1 embryos produced by mosaic breeders were genotyped individually and 3 pairs of founder adult fish (F0) with 3 different substitutions of c.386C were identified: c.386C>T p.Ser129Phe, c. 386C>A p.Ser129Tyr, and c.386C>G p.Ser129Cys. The c.386C>T p.Ser129Phe fish also carried a second, silent variant, c.384C>T p.Ala128Ala. For genotyping, DNA was first amplified with primers flanking the target site: 5'- aacagaatgcatatatttgtgtttcc and 5'- tctacttgttaagctgcaaattctc and then the resulting DNA fragment was either sequenced or digested with the BsaXI restriction enzyme (NEB).

The same modified CRISPR-Cas9 system was also used to generate zebrafish with a 24 base pair deletion, c.377_396+4del, across the *wdr37* exon5/intron5 junction. Another line harboring a c.484_491del variant was produced with conventional *S. pyogenes* Cas9 endonuclease and gRNA (5'- GGAGAAGGACAGACAGTCGA) targeting *wdr37* exon4. Genotyping was done by amplification of the DNA fragment containing the targeted site with 5'- ccaaagacttgtcctgcatt and 5'- tcagccctattcactcgaca primers and restriction digestion with the AhdI enzyme (NEB).

Zebrafish produced by mosaic founders were collected at different stages (5-7 dpf, 9-14 dpf, 17-19 dpf, 1 month, 2-3 months), observed for phenotypes and genotyped for the alleles described above. The percent of heterozygous animals for each allele at different ages (5-7- dpf, 9-14-dpf, 17-19-dpf, and over 1 month (30+ dpf)) was identified and statistical significance was calculated using a Chi-square 2x2 contingency table test to compare each group of fish.

Zebrafish were observed and imaged using a Zeiss Discovery V12 microscope. Embryos were maintained in petri dishes in standard medium in an incubator at 28.5°C up to 5-6 dpf. Then the embryos were placed onto a recirculating aquatic system (Aquatic Habitats) to grow into adults; zebrafish larvae were collected at the stages indicated above for observations and genotyping. Total body length (from the tip of the maxilla to the tip of the tail) and head size (from the tip of the maxilla to the center of the otic vesicle) measurements were taken using lateral fish images and the resultant data were used to calculate mean and standard deviation values for wild-type and each mutant; the head size measurement was divided by body length to calculate a head-to-body ratio. Statistical significance for all comparisons was determined using a t-test.

RNA extraction and RNA-seq

Five-day-old zebrafish embryos from a cross of two mosaic F0 parents were anesthetized with tricaine methanesulfonate (Sigma) in Ringer buffer. Tails were removed for genotyping, and each embryo was placed in an individual tube and lysed in TRI reagent (Zymo Research). DNA from the tails was extracted by alkaline lysis[8] by incubation in 50mM NaOH at 95°C for 15 minutes with subsequent neutralization with 1/10 of the volume of 1M Tris HCl, pH 8.0. Genotyping was performed as described above and embryos heterozygous for the c.386C>T p.Ser129Phe variant or wild-type at this site were identified. Three independent RNA samples were prepared with each sample containing RNA from five individual embryos pooled together using Direct-zol™ RNA MiniPrep kit (Zymo Research). RNA from mutant and wild-type embryos was submitted to Macrogen for sequencing. All sequenced samples were assessed for quality and had an RNA Integrity Number (RIN) greater than 7.0. Whole transcriptome sequencing on 6 paired-ends samples was performed utilizing TruSeq RNA Sample Prep Kit v2 on the Illumina HiSeq X Ten platform. Reads obtained from RNA sequencing were mapped to the Danio rerio reference genome GRCz11. Bioinformatic analysis performed by Macrogen included FastQC v0.11.7 to perform quality check on the raw sequences, Trimmomatic 0.38 for trimming of the sequences, HISAT2 version 2.1.0, Bowtie2 2.3.4.1 for mapping next-generation sequencing reads to genomes, and StringTie version 1.3.4d to assemble RNA-Seq alignments. DEG (Differentially Expressed Genes) analysis was performed to compare the mutant and wild-type transcriptome using DESeq2. The averaged FPKM (Fragments Per Kilobase of transcript per Million mapped reads) values ratio were analyzed for transcripts which had changed at least 2 folds in either direction. The results showed 145 genes which satisfied |fc|>=2 & nbinomWaldTest raw p-value<0.05 conditions in comparison pair. No secondary validation of the identified differentially expressed transcripts was performed. Predicted activity of the pathways based on the fold changes of the averaged FPKM was determined by Ingenuity Pathway Analysis (IPA) (QIAGEN). Full RNAseq data are available in the ArrayExpress database at EMBL-EBI (www.ebi.ac.uk/arrayexpress; Accession number E-MTAB-8029.

References

1. Weh, E., Reis, L.M., Happ, H.C., Levin, A.V., Wheeler, P.G., David, K.L., Carney, E., Angle, B., Hauser, N., and Semina, E.V. (2014). Whole exome sequence analysis of Peters anomaly. Human genetics 133, 1497-1511.
2. Weh, E., Reis, L.M., Tyler, R.C., Bick, D., Rhead, W.J., Wallace, S., McGregor, T.L., Dills, S.K., Chao, M.C., Murray, J.C., et al. (2014). Novel B3GALTL mutations in classic Peters plus syndrome and lack of mutations in a large cohort of patients with similar phenotypes. Clinical genetics 86, 142-148.

3. MyGene2. NHGRI/NHLBI University of Washington-Center for Mendelian Genomics (UW-CMG). In. (Seattle, WA

4. Yang, J., Yan, R., Roy, A., Xu, D., Poisson, J., and Zhang, Y. (2015). The I-TASSER Suite: protein structure and function prediction. Nat Methods 12, 7-8.

5. Sorokina, E.A., Muheisen, S., Mlodik, N., and Semina, E.V. (2011). MIP/Aquaporin 0 represents a direct transcriptional target of PITX3 in the developing lens. PLoS One 6, e21122.

6. Zhang, Y., Qin, W., Lu, X., Xu, J., Huang, H., Bai, H., Li, S., and Lin, S. (2017). Programmable base editing of zebrafish genome using a modified CRISPR-Cas9 system. Nat Commun 8, 118.

7. Hwang, W.Y., Fu, Y., Reyon, D., Maeder, M.L., Tsai, S.Q., Sander, J.D., Peterson, R.T., Yeh, J.R., and Joung, J.K. (2013). Efficient genome editing in zebrafish using a CRISPR-Cas system. Nat Biotechnol 31, 227-229.

8. Meeker, N.D., Hutchinson, S.A., Ho, L., and Trede, N.S. (2007). Method for isolation of PCR-ready genomic DNA from zebrafish tissues. Biotechniques 43, 610, 612, 614.